Cellular homeostasis in the *Drosophila* retina requires the lipid phosphatase Sac1

Nigel W. Griffiths[a,b], Lauren M. Del Bel[a,b], Ronit Wilk[a], and Julie A. Brill[a,b,*]

[a]Cell Biology Program, The Hospital for Sick Children, Toronto, ON M5G 0A4, Canada; [b]Department of Molecular Genetics, University of Toronto, Toronto, ON M5S 1A8, Canada

ABSTRACT The complex functions of cellular membranes, and thus overall cell physiology, depend on the distribution of crucial lipid species. Sac1 is an essential, conserved, ER-localized phosphatase whose substrate, phosphatidylinositol 4-phosphate (PI4P), coordinates secretory trafficking and plasma membrane function. PI4P from multiple pools is delivered to Sac1 by oxysterol-binding protein and related proteins in exchange for other lipids and sterols, which places Sac1 at the intersection of multiple lipid distribution pathways. However, much remains unknown about the roles of Sac1 in subcellular homeostasis and organismal development. Using a temperature-sensitive allele (*Sac1[ts]*), we show that Sac1 is required for structural integrity of the *Drosophila* retinal floor. The β_{ps}-integrin Myospheroid, which is necessary for basal cell adhesion, is mislocalized in *Sac1[ts]* retinas. In addition, the adhesion proteins Roughest and Kirre, which coordinate apical retinal cell patterning at an earlier stage, accumulate within *Sac1[ts]* retinal cells due to impaired endo-lysosomal degradation. Moreover, Sac1 is required for ER homeostasis in *Drosophila* retinal cells. Together, our data illustrate the importance of Sac1 in regulating multiple aspects of cellular homeostasis during tissue development.

INTRODUCTION

Although they comprise a minor fraction of total cellular phospholipid content, phosphoinositides, also known as phosphatidylinositol phosphates (PIPs), act as essential coordinators of membrane function and identity (Balla, 2013). PIPs are derived from the precursor phosphatidylinositol, whose inositol head group can be phosphorylated at any of three positions to yield seven unique PIP species that recruit distinct sets of effector proteins. Through the localized activity of PIP kinases and phosphatases, these species are interconverted to maintain enrichment in different membranes and to regulate numerous PIP effector-driven processes (Balla, 2013).

Sac1 is a conserved phosphatase whose substrate, phosphatidylinositol 4-phosphate (PI4P), coordinates multiple stages in secretory trafficking, participates in cellular signaling pathways, and acts as the precursor for $PI(4,5)P_2$ at the plasma membrane (PM) (Graham and Burd, 2011; Tan and Brill, 2014; Del Bel and Brill, 2018). PI4P is produced in the PM and Golgi, respectively, by two conserved type III PI 4-kinases (PI4Ks), PI4KIIIα (Balla *et al.*, 2005; Baird *et al.*, 2008; Yan *et al.*, 2011; Nakatsu *et al.*, 2012; Tan *et al.*, 2014), and PI4KIIIβ (Godi *et al.*, 1999; Walch-Solimena and Novick, 1999; Brill *et al.*, 2000; Polevoy *et al.*, 2009). In addition, a type II PI4K (PI4KIIα) produces PI4P in the *trans*-Golgi network (TGN) (Wang *et al.*, 2003; Minogue *et al.*, 2010) and on endosomes, where it is important for endosomal trafficking (Balla *et al.*, 2002; Salazar *et al.*, 2005; Minogue *et al.*, 2006; Burgess *et al.*, 2012; Jovic *et al.*, 2012; Ma *et al.*, 2020).

In contrast to the distribution of PI4Ks and PI4P, Sac1 localizes primarily to the ER, as well as the *cis*-Golgi under growth-limiting conditions (Faulhammer *et al.*, 2005, 2007; Blagoveshchenskaya *et al.*, 2008). Although seemingly capable of acting in *trans* on PI4P in neighboring membranes in some scenarios (Manford *et al.*, 2010; Stefan *et al.*, 2011; Venditti *et al.*, 2019a), Sac1 appears to predominantly depend on delivery of PI4P to the ER via nonvesicular lipid transport at membrane contact sites (MCS) (Chung *et al.*, 2015; Mesmin *et al.*, 2017; Pietrangelo and Ridgway, 2018). For instance, oxysterol-binding protein (OSBP), which localizes to ER–*trans*-Golgi MCS through interactions with the ER-resident vesicle-associated membrane protein-associated protein VAP as well as PI4P in the *trans*-Golgi, delivers PI4P from the *trans*-Golgi to the ER in exchange for sterols (Levine and Munro, 2002; Wyles *et al.*, 2002; Loewen *et al.*, 2003; Lev, 2010). Hydrolysis of incoming PI4P by Sac1 maintains a low concentration of PI4P in the ER that is necessary for sustained PI4P/sterol countertransport in vitro, although this relationship appears more nuanced in vivo (Mesmin *et al.*, 2013; Charman *et al.*, 2017). OSBP-related proteins (ORPs), which are encoded by 11 genes in humans and three in flies (Lehto *et al.*, 2001; Fairn and McMaster, 2008; Ma *et al.*, 2010), function similarly to OSBP but differ in their localization and lipid-binding preferences. Despite its essential function, how Sac1 regulates different aspects of cellular homeostasis during animal development is not fully understood.

In *Drosophila*, null *Sac1* mutants exhibit embryonic lethality due to defects in cell shape and ectopically activated JNK signaling that prevent dorsal closure (Wei *et al.*, 2003a). JNK signaling defects are also observed in *Sac1* clones in larval imaginal discs (Yavari *et al.*, 2010). Moreover, Sac1 regulates Hedgehog signaling by inhibiting recruitment and activation of Smoothened at the PM in a PI4P-dependent manner (Yavari *et al.*, 2010; Jiang *et al.*, 2016). Sac1 is also required for axonal pathfinding in the embryonic central nervous system, as well as for axonal transport and synaptogenesis in larval neurons (Lee *et al.*, 2011; Forrest *et al.*, 2013).

In addition, loss of Sac1 causes severe tissue disorganization and degeneration during eye development (Wei *et al.*, 2003b). The *Drosophila* eye is composed of ~750 unit eyes called ommatidia. Presumptive ommatidia arise early in pupal development, where they initially comprise clusters of medial/basal photoreceptors and apical cone cells surrounded by a disordered pool of undifferentiated interommatidial cells (IOCs) (Ready *et al.*, 1976; Tomlinson, 1985; Tomlinson and Ready, 1987; Cagan and Ready, 1989). During the first half of the ~96-h pupal stage, two IOCs per ommatidium differentiate into primary pigment cells (1°pc), which encircle the cone cells. The remaining IOCs subsequently differentiate into a lattice of secondary and tertiary pc (2°/3°pc) and sensory bristles that separate neighboring ommatidia or are removed by apoptosis by 42 h after puparium formation (APF) (Cagan and Ready, 1989; Wolff and Ready, 1991). Changes in IOC shape and position during this stage require the Irre cell recognition module (IRM) adhesion proteins Roughest (Rst) and Hibris (Hbs), as well as their paralogues Kirre and Sticks and stones (Sns) (Reiter *et al.*, 1996; Bao and Cagan, 2005; Bao *et al.*, 2010). Rst/Kirre and Hbs/Sns are orthologues of mammalian Neph1 and nephrin, which are needed for formation of the renal slit diaphragm (Ruotsalainen *et al.*, 1999; Tryggvason, 1999; Donoviel *et al.*, 2001; Helmstädter *et al.*, 2014) as well as during myoblast fusion (Bour *et al.*, 2000; Ruiz-Gómez *et al.*, 2000; Artero *et al.*, 2001; Strünkelnberg *et al.*, 2001; Sohn *et al.*, 2009). After IOC patterning, during late stages of pupal eye development (42–96 h APF), the retina elongates fivefold (Longley and Ready, 1995), and laminated corneal lenses with underlying gelatinous pseudocones are secreted (Cagan and Ready, 1989), giving the eye its characteristic adult appearance.

We previously examined the role of Sac1 in the developing *Drosophila* eye using a hypomorphic *Sac1* allele that is temperature sensitive (*Sac1ts*) (Wei *et al.*, 2003b; Del Bel *et al.*, 2018). *Sac1ts* flies develop morphologically normal eyes when reared at 18°C, but display a rough eye phenotype caused by defective IOC sorting when reared at or above 23.5°C. Here, we show that *Sac1ts* eyes exhibit structural defects at the retinal floor and mislocalization of the β_{ps}-integrin Myospheroid (Mys), which is required for retinal floor adhesion (Zusman *et al.*, 1993; Longley and Ready, 1995). This defect is not due to a loss of cell polarity, as apical adherens junctions are unaffected. However, we identified a novel secondary defect in the distribution of Rst and Kirre, which are apical transmembrane proteins. At 42 h APF, *Sac1ts* 2°/3°pc contain an excess of intracellular Rst and Kirre due to impaired endo-lysosomal trafficking and degradation. *Sac1ts* 2°/3°pc also accumulate PI4P and F-actin on enlarged, basal endosomes and exhibit ER stress. Thus, we have identified novel roles for Sac1 in regulating cellular homeostasis during tissue morphogenesis.

RESULTS

Sac1 loss leads to retinal floor breakdown

Sac1ts flies exhibit reduced viability and a rough eye phenotype when raised at or above 23.5°C (Wei *et al.*, 2003b; Del Bel *et al.*, 2018). We examined longitudinal sections of adult eyes from flies raised at 23.5°C using light microscopy and transmission electron microscopy (TEM) and discovered severe structural defects in the basal region of *Sac1ts* ommatidia (Figure 1). This region, known as the retinal floor, includes a layer of 2°/3°pc feet, a basal lamina, and a subretinal pigment layer (Cagan and Ready, 1989; Tomlinson, 2012). The 2°/3°pc feet lie on top of the basal lamina, creating a fenestrated membrane and forming "grommets" of focal adhesions that support photoreceptor cells and provide exit ports for axon projection to the brain (Longley and Ready, 1995). In wild-type (WT) adult eyes, the fenestrated membrane was complete, and the subretinal pigment layer was contiguous and directly adjacent to the brain (Figure 1, A and D). In contrast, in *Sac1ts* adult eyes, the fenestrated membrane appeared broken, the subretinal pigment layer was missing, and a gap was observed between the retinal floor and the brain (Figure 1, B and E, asterisks). *Sac1ts* adult eyes also exhibited other notable morphological defects, such as extensive vacuolization throughout ommatidia that were not observed in WT eyes (Figure 1B, blue asterisks).

In addition to structural defects at the retinal floor, *Sac1ts* ommatidia are stunted compared with WT ommatidia. A comparison of the lengths (Figure 1, A and B, blue lines) of individual ommatidia revealed that the average ommatidial length for *Sac1ts* mutants was 64% of WT (Figure 1C; $n = 26$ ommatidia, $p < 1 \times 10^{-17}$). Thus, the architecture of the retinal floor as well as ommatidial dimensions were severely affected in *Sac1ts* mutants raised at 23.5°C.

Mys is disorganized in *Sac1ts* 2°/3°pc

Drosophila pupal eye development can be divided into two main stages: (1) an early stage where retinal precursor cells are patterned and subsequently specified (0–42 h APF) (Figure 1F) and (2) a later stage where retinal elongation occurs and cells produce specialized structures, including rhabdomeres, bristles, and pigment granules (~42–96 h APF) (Cagan and Ready, 1989).

Retinal elongation requires proper retinal floor adhesion, which is mediated by the β_{ps}-integrin Mys (Zusman *et al.*, 1993; Longley and Ready, 1995). Without Mys, 2°/3°pc feet do not adhere to the underlying basement membrane; as the retina elongates, the feet pull away from the basement membrane creating an observable
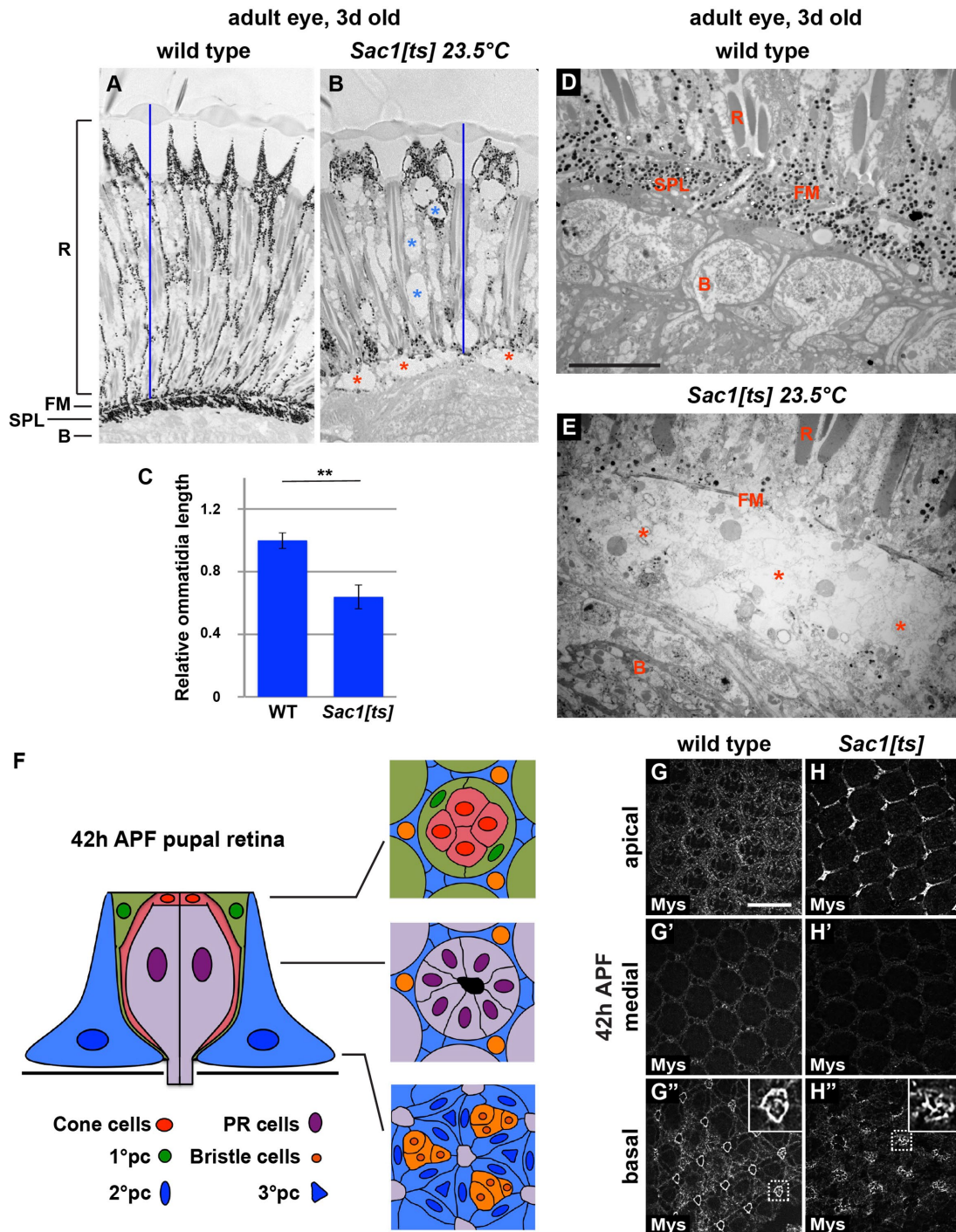
FIGURE 1: Sac1 is required for retinal floor organization. (A, B) Micrographs of eyes from 3-d-old flies raised at 23.5°C showing a longitudinal view through the ommatidia. $Sac1^{ts}$ mutants display a highly disorganized retinal floor (B, red asterisks) and extensive vacuolization (B, blue asterisks) compared with WT (A). (C) Quantification of average ommatidial length in WT and $Sac1^{ts}$. Values are normalized to WT. Error bars represent SD; $n = 26$ ommatidia. **$p < 1 \times 10^{-17}$, two-tailed Student's t test. (D, E) TEM of 3-d-old adult fly eyes showing the retinal floor. $Sac1^{ts}$ mutants exhibit a gap between the retinal floor and the brain (E, red asterisks), which is absent in WT (D). R, retina; FM, fenestrated membrane; SPL, subretinal pigment layer; B, brain. Scale bar: 10 μm. (F) Schematic showing longitudinal view through a single pupal ommatidium illustrating retinal cell organization at 42 h APF. Cross-sections through a single ommatidium at different optical planes (apical, medial, basal) are shown to the right. Apical: cone cells (pale red) and 1°pc (light green) are surrounded by a lattice of 2°/3°pc (blue) and bristles (orange). Cone cell and 1°pc nuclei localize apically. Medial: photoreceptor (PR) cells (light purple) and their developing rhabdomeres (denoted in black) are visible. PR cell nuclei localize medially (dark purple). Basal: PR cells project to the brain (light purple), 2°/3°pc feet lie along the retinal floor, and bristle cell bodies are located in basal regions of the retina, yielding the characteristic "flower pattern" (Wolff and Ready, 1991). 2°/3°pc and bristle cell nuclei localize basally (dark blue and dark orange). (G–H") Apical, medial, and basal confocal sections of WT and $Sac1^{ts}$ retinas at 42 h APF stained for the $β_{PS}$-integrin Mys. Insets in G" and H" are magnified threefold. Scale bar: 15 μm.

gap and yielding stunted (i.e., shorter and wider) ommatidia (Zusman *et al.*, 1993; Longley and Ready, 1995). Because *Sac1^ts* mutants exhibited a similar gap between the retinal floor and the brain (Figure 1, B and E, red asterisks), we examined Mys distribution at the retinal floor (i.e., basally) in *Sac1^ts* mutants. In WT, as expected, Mys was highly enriched at the grommets where 2°/3°pc feet converge (Figure 1G", inset) (Longley and Ready, 1995). In contrast, in *Sac1^ts* mutants, Mys grommet enrichment was lost (Figure 1H", inset). Furthermore, whereas in apical-medial regions of WT retinas Mys was present in small puncta within 2°/3°pc and along 2°/3°pc membranes (Figure 1, G and G'), in *Sac1^ts* retinas Mys appeared similar to WT in medial sections but accumulated intracellularly within 2°/3°pc in apical regions (Figure 1, H and H').

To assess whether Mys accumulates apically in *Sac1^ts* due to defects in cell polarity, we examined the apical cell surface markers DE-Cadherin (DE-Cad), Discs large (Dlg), and Armadillo (Arm) at 42 h APF (Supplemental Figure S1). DE-Cad localized to apical cell borders normally in *Sac1^ts* retinas and, although there were slight differences in medial-basal distribution (likely a consequence of structural defects at the retinal floor), *Sac1^ts* 2°/3°pc did not accumulate DE-Cad intracellularly, as seen with Mys (Supplemental Figure S1, A–B"). Similarly, Dlg and Arm were unaffected in *Sac1^ts* 2°/3°pc compared with WT (Supplemental Figure S1, C–F"). Thus, Sac1 is essential for maintaining organization and integrity of the retinal floor at 42 h APF, but not for maintaining adherens junctions and apical polarity. Sac1 loss leads to Mys disorganization at 2°/3°pc feet, which likely prevents 2°/3°pc feet from properly adhering to the basal lamina, resulting in gross morphological defects in the adult eye following retinal elongation (Figure 1, B and E).

Loss of Sac1 leads to IRM protein accumulation in 2°/3°pc

In addition to junctional proteins, we analyzed other apical cell surface proteins and discovered a defect in the distribution of the IRM adhesion proteins Rst and Kirre at 42 h APF (Figure 2, A–H). Earlier in pupal development, during IOC positioning, Rst and Kirre are expressed in IOCs, while their binding partners Hbs and Sns are expressed in 1°pc (Reiter *et al.*, 1996; Bao and Cagan, 2005; Bao *et al.*, 2010). The resulting adhesion at apical IOC:1°pc borders moves IOCs into single file at 24 h APF, which is necessary for downstream patterning of 2°/3°pc and sensory bristles (Bao and Cagan, 2005). From 24–42 h APF, Rst and Kirre are transcriptionally downregulated and gradually removed from apical IOC PMs (Araujo *et al.*, 2003; Machado *et al.*, 2011). In WT retinas, we observed little Rst or Kirre at apical cell borders or intracellularly at 42 h APF (Figure 2, A, C, E, and G). In *Sac1^ts* retinas, although Rst and Kirre were largely absent from apical regions (with the exception of bristle cells, which accumulate Kirre similar to WT) (Figure 2B), the two proteins accumulated in large intracellular puncta in medial and basal regions of 2°/3°pc (Figure 2, D, F, and H). Partial colocalization was observed between Rst and Kirre in *Sac1^ts*, suggesting that these proteins localize to the same intracellular compartment (Figure 2, D' and F', white, and H, merge). Notably, we observed a similar accumulation of Notch in *Sac1^ts*, indicating that this phenotype affects transmembrane proteins other than Rst and Kirre (Supplemental Figure S2). Expression of a WT Sac1 transgene (*mCh-Sac1(WT)*) rescued the Rst protein accumulation defect in *Sac1^ts* mutants (Figure 2I), whereas expression of a phosphatase-reduced (PR) Sac1 transgene (*mCh-Sac1(PR)*) did not (Figure 2J). Thus, catalytic activity of Sac1 is required for IRM protein regulation.

To determine if IRM protein accumulation was due to a developmental delay, we generated clones of retinal cells homozygous mutant for *Sac1^ts* using FLP/FRT-mediated recombination

(Xu and Rubin, 1993). *Sac1^ts* mutant clones (GFP-negative) exhibited Rst accumulation within 2°/3°pc (GFP-positive), while adjacent WT 2°/3°pc lacked Rst staining (Figure 2K). Hence, accumulation of Rst and Kirre in *Sac1^ts* 2°/3°pc at 42 h APF is not due to a developmental delay, but rather due to a cell-intrinsic requirement for Sac1.

We also examined Rst distribution in WT and *Sac1^ts* retinas at 30 h APF and 36 h APF to gain a better sense of the timing of IRM protein accumulation. At 30 h APF, Rst puncta in medial and basal sections of *Sac1^ts* 2°/3°pc were already more noticeable than in WT (Supplemental Figure S3, A–B"). By 36 h APF, basal Rst accumulation in *Sac1^ts* had progressed even further (Supplemental Figure S3, C–D"). IRM protein accumulation therefore occurs progressively from at least as early as 30 h APF up to 42 h APF.

Loss of Sac1 induces ER stress and UPR in 2°/3°pc

Accumulation of Rst and Kirre in *Sac1^ts* mutants could be a consequence of protein misfolding and retrotranslocation from the ER, improper protein secretion or recycling at the PM, or altered protein degradation. VAP, which recruits OSBP to the ER to deliver PI4P to Sac1, is important for ER homeostasis in *Drosophila* (Tsuda *et al.*, 2008; Moustaqim-Barrette *et al.*, 2014). Moreover, in yeast, loss of Sac1 impedes protein folding and trafficking of newly synthesized proteins out of the ER (Mayinger *et al.*, 1995; Kochendorfer *et al.*, 1999). Thus, we first examined the effect of *Sac1^ts* on the ER.

To determine whether Kirre accumulates in the ER, we examined its association with the ER retention signal KDEL. In both WT and *Sac1^ts* retinas, we did not observe colocalization between Kirre and KDEL (Figure 3, A–B'; Supplemental Figure S4). However, *Sac1^ts* retinas contained enlarged KDEL-positive structures in basal regions that were absent in WT retinas (Figure 3, A–B'). This suggested that ER resident proteins might not be properly retained in the ER or that ER membranes are expanded, raising the possibility that *Sac1^ts* 2°/3°pc experience ER stress. To test this, we examined the distribution of the ER chaperone BiP, which is up-regulated in response to ER dysfunction as part of the unfolded protein response (UPR) (Lee, 2005; Otero *et al.*, 2010). In basal regions of WT retinas, BiP was strongly expressed in bristle cells surrounding the bristle cell nuclei (Figure 3, C and C', arrows), but not in adjacent 2°/3°pc. Meanwhile, in *Sac1^ts* retinas, bristle cells were difficult to discern and BiP expression was seen in 2°/3°pc, surrounding 2°/3°pc nuclei at the retinal floor (Figure 3, D and D').

We confirmed that *Sac1^ts* 2°/3°pc experience ER stress using an Xbp1-GFP reporter that is spliced, translated, and translocated to the nucleus when the ER stress sensor IRE1 is activated (Sone *et al.*, 2013). WT and *Sac1^ts* retinas were stained with DAPI to visualize nuclei and monitored for GFP expression at 42 h APF. In apical regions of WT and *Sac1^ts* retinas, where cone cell and 1°pc nuclei are located, there was little detectable Xbp1-GFP, indicating that these cells were largely unstressed (Figure 4, A and B). In medial regions, Xbp1-GFP could be seen in both WT and *Sac1^ts* photoreceptor nuclei, indicating that photoreceptor cells experience ER stress, as previously reported (Coelho *et al.*, 2013) (Figure 4, C and D). In basal regions, where 2°/3°pc nuclei are located, Xbp1-GFP was present in the majority of *Sac1^ts* 2°/3°pc nuclei and absent from WT 2°/3°pc nuclei (Figure 4, E and F). Thus, Sac1 loss induces ER stress and UPR in 2°/3°pc.

Rst does not colocalize with the autophagy adaptor Ref(2)P

When ER function is compromised, UPR is induced to increase ER protein folding capacity and remove misfolded proteins. As part of this response, proteins that are unable to fold are retrotranslocated from the ER to the cytosol, where they are ubiquitinated and degraded (ER-associated degradation; ERAD) (Fujita *et al.*, 2007;
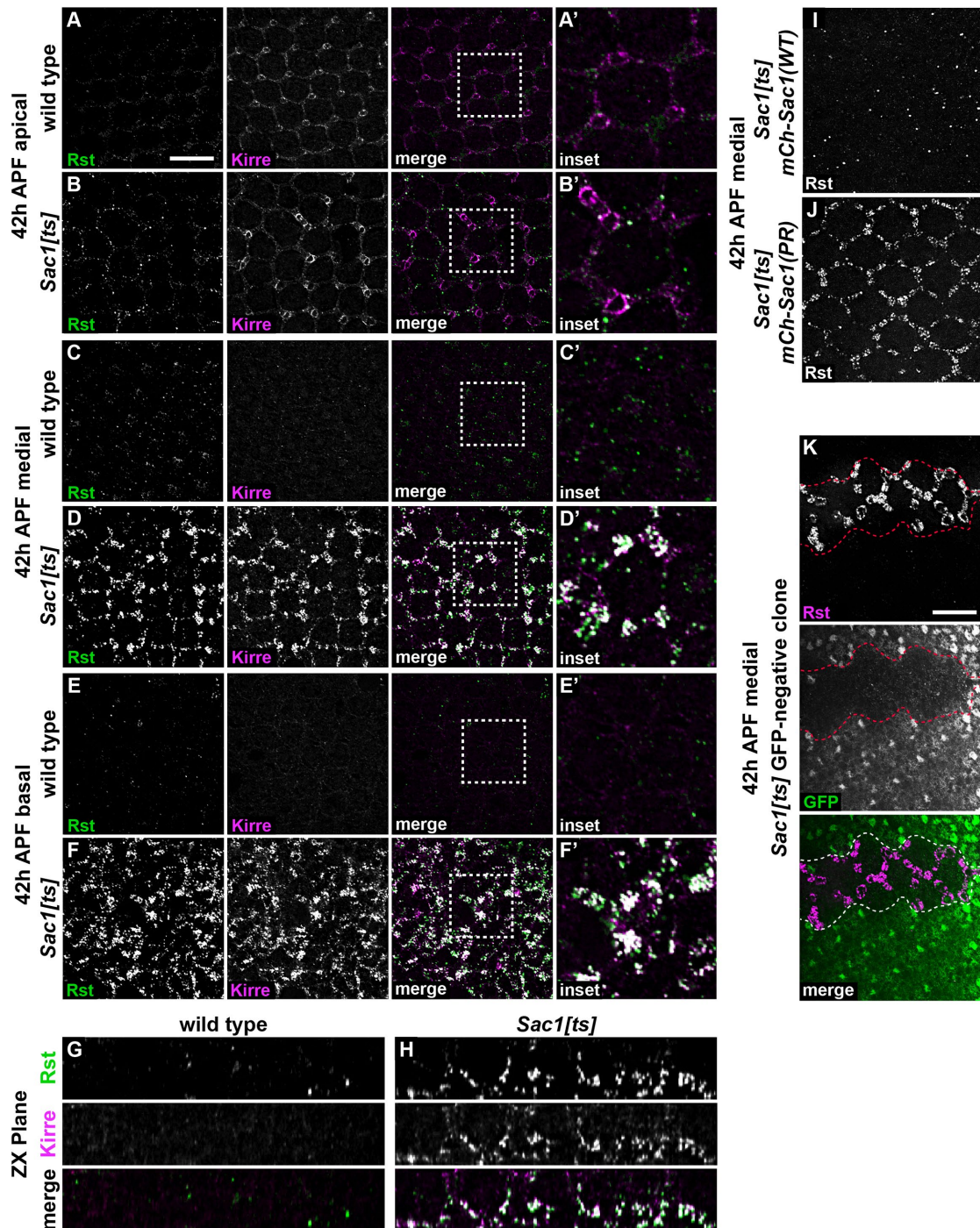
FIGURE 2: *Sac1[ts]* 2°/3°pc accumulate the IRM proteins Rst and Kirre. (A–H) Confocal sections of pupal retinas at 42 h APF stained for Rst (green) and Kirre (magenta). White in merged images indicates colocalization. Boxed regions are magnified twofold in insets (A'–F'). (G, H) Optical views of the longitudinal ZX plane clearly show medial-basal accumulation of Rst and Kirre in *Sac1[ts]* mutants at 42 h APF (H). (I, J) Medial confocal sections of 42 h APF retinas stained for Rst. Expression of *mCh-Sac1(WT)* rescues Rst protein accumulation in *Sac1[ts]* mutants (I), while expression of *mCh-Sac1(PR)* does not (J). (K) *Sac1[ts]* mutant clone stained for Rst (magenta). Mutant clone is GFP-negative and outlined by a red or white dashed line. Scale bars: 15 μm.

Araki and Nagata, 2011; Houck and Cyr, 2012). In *Drosophila* neurons, loss of VAP causes UPR induction and accumulation of ubiquitinated proteins (Tsuda *et al.*, 2008; Moustaqim-Barrette *et al.*, 2014). Given that *Sac1[ts]* 2°/3°pc also display UPR activation, we thus investigated whether Rst and Kirre accumulate in the cytosol as ERAD substrates.

In the cytosol, ubiquitinated protein aggregates are targeted to autophagosomes by the adaptor protein Ref(2)P (p62 in mammals) (Bjørkøy *et al.*, 2005; Wooten *et al.*, 2006; Nezis *et al.*, 2008; Houck and Cyr, 2012). To determine if Rst aggregates in *Sac1[ts]* are targets of autophagy, we examined the distribution of Ref(2)P as well as mono-/poly-ubiquitin. We did not observe a change in the pattern
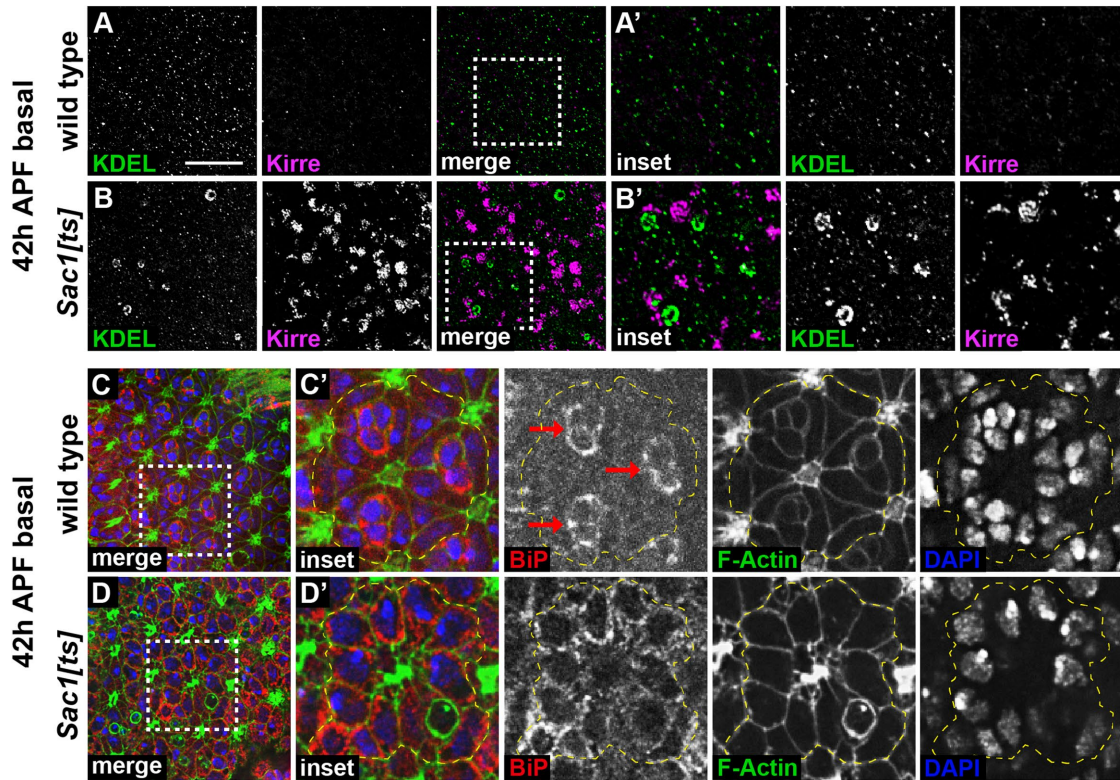
FIGURE 3: *Sac1ts* 2°/3°pc exhibit basal ER expansions and up-regulation of BiP. (A-B') Basal confocal sections of WT and *Sac1ts* pupal retinas at 42 h APF costained for KDEL (green) and Kirre (magenta). *Sac1ts* 2°/3°pc display Kirre accumulation and enlarged KDEL-positive structures. (C–D') Basal confocal sections of WT and *Sac1ts* retinas at 42 h APF stained for BiP (red), F-actin (green), and DNA (DAPI, blue). In WT, F-actin is highly organized, 2°/3°pc and bristle cell nuclei are compact and well ordered, and BiP is expressed only in bristle cells (C, C', arrows). In contrast, in *Sac1ts*, F-actin is disorganized, bristle cells are difficult to discern, 2°/3°pc nuclei are less compact, and BiP expression is up-regulated in 2°/3°pc (D, D'). Dashed yellow lines outline ommatidia. Boxed regions are magnified twofold in the insets (A'–F'). Scale bar: 15 μm.

of ubiquitination compared with WT in medial-basal regions of *Sac1ts* 2°/3°pc where Rst and Kirre accumulate (Figure 5, A–B'). Similarly, Ref(2)P did not colocalize with Rst aggregates in *Sac1ts* (Figure 5, C–D'), although we did observe an apparent increase in Ref(2)P abundance compared with WT, which could indicate a delay in autophagic protein turnover (Figure 5, compare A and C to B and D). Therefore, Rst puncta do not appear to be targets of autophagy in *Sac1ts* retinas at 42 h APF, as would be expected if they were cytosolic aggregates.

We also tested whether chemically inducing ER stress using DTT in WT retinas cultured ex vivo causes Rst accumulation that resembles *Sac1ts*. Treatment with concentrations of DTT high enough to induce Xbp1-GFP expression after 4 h in culture caused a visible reduction in Rst abundance, indicating that ER stress is not sufficient to induce Rst accumulation (Supplemental Figure S5). Taken together, these results suggest that although 2°/3°pc experience ER stress in *Sac1ts*, ERAD does not cause Rst aggregation.

Rst partially colocalizes with YFP-Rab7 in *Sac1ts* 2°/3°pc

Having found no evidence that ER stress causes Rst and Kirre aggregation in the ER or cytosol, we wondered whether these proteins accumulate due to failed anterograde trafficking or endosomal degradation. Therefore, to identify where these transmembrane proteins accumulate within *Sac1ts* 2°/3°pc at 42 h APF and to uncover possible defects in protein trafficking or degradation, we examined markers of various subcellular compartments, including the Golgi

(Lava lamp, Lva), recycling endosomes (Rab11), the exocyst complex (Sec8), early endosomes (Rab5), late endosomes (YPF-Rab7 and Syntaxin7, Syx7), and lysosomes (Arl8) (Figure 6). In both WT and *Sac1ts*, we observed no colocalization of Rst or Kirre with Lva, Rab11, or Sec8 (Figure 6, A–F), indicating that these proteins do not accumulate in the Golgi, recycling endosomes, or exocytic compartments. In WT, Rst colocalized in rare puncta with Rab5 (Figure 6G), YFP-Rab7 (Figure 6I), and Arl8 (Figure 6M). This is consistent with the idea that Rst and Kirre are removed from apical 2°/3°pc membranes by endocytosis during later stages of pupal eye development (Araujo *et al.*, 2003; Machado *et al.*, 2011). Rst did not accumulate within Rab5-positive endosomes or Arl8-positive lysosomes in *Sac1ts* retinas (Figure 6, H and N). However, *Sac1ts* mutants did show notable colocalization of Rst with YFP-Rab7 (Figure 6J), as well as with Syx7 (Figure 6L). This suggested that Rst and Kirre might accumulate in late endosomes due to a delay in endo-lysosomal trafficking or degradation.

Endosomal Rst trafficking and degradation is delayed in *Sac1ts* 2°/3°pc

To test whether endocytic trafficking and degradation of internalized Rst is indeed delayed in *Sac1ts* 2°/3°pc, we performed a pulse-chase antibody uptake and degradation assay. WT and *Sac1ts* retinas were dissected in culture medium at 28 h APF, incubated in medium containing anti-Rst and anti-Lva primary antibodies at 25°C for 15 min, then washed and cultured at 25°C for an additional
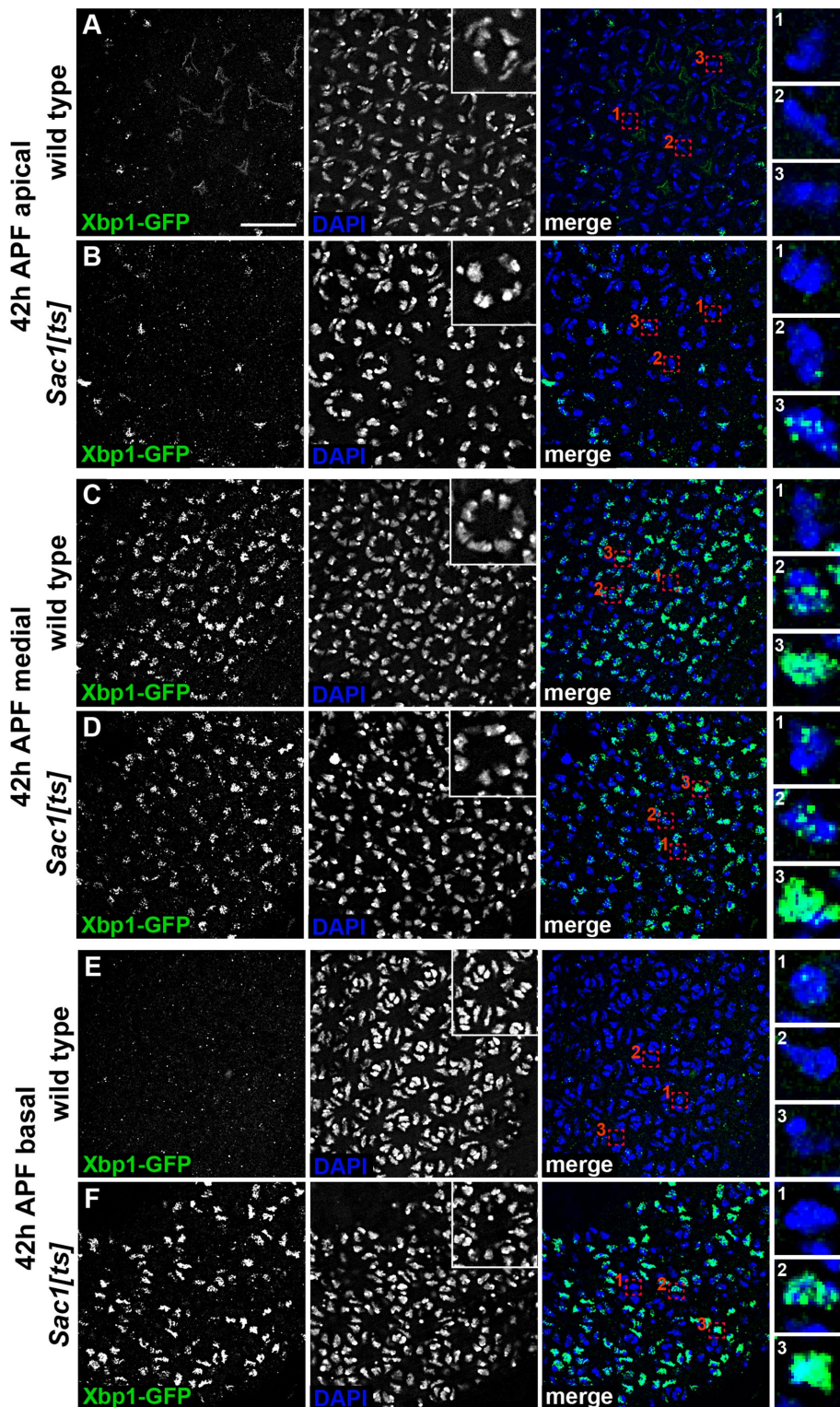
FIGURE 4: Loss of Sac1 induces ER stress and UPR in 2°/3°pc. (A–F) Confocal sections of WT and *Sac1ts* retinas expressing the Xbp1-GFP reporter (green) and stained for DNA (DAPI, blue) at 42 h APF. Boxed regions outlined in red highlight individual nuclei that are magnified fivefold in numbered insets. In apical sections, WT cone cell nuclei lack the Xbp1-GFP reporter (A), whereas small amounts of Xbp1-GFP are observed in a subset of *Sac1ts* cone cell nuclei (B). In medial sections, Xbp1-GFP is present in photoreceptor cell nuclei in both WT (C) and *Sac1ts* (D). In basal sections (E, F), where 2°/3°pc nuclei are located, Xbp1-GFP is nuclear only in *Sac1ts* retinas, indicating that *Sac1ts* 2°/3°pc experience ER stress. Scale bar: 15 µm.

45 min, or 3 h 45 min (in parallel in the same experiment) before being fixed and permeabilized for secondary antibody staining. Culturing was performed over the span of 28–32 h APF, when there is still ample Rst present at the apical PM yet Rst accumulation in *Sac1ts* has already begun.

We examined single optical sections as well as extended projections of serial optical sections taken from the apical to basal surfaces of representative WT and *Sac1ts* retinas (Figure 7, A–T'). After the 45-min chase, bright Rst puncta were present throughout 2°/3°pc of *Sac1ts* and WT retinas, while some antibody-labeled Rst remained at the apical PM (Figure 7, A–H', Q–R'). The overall number of Rst-positive puncta per ommatidium between WT and *Sac1ts* was not significantly different, indicating the dynamics of Rst uptake were initially similar between genotypes (Figure 7U; n = 104 ommatidia). No Lva staining was detected, indicating the tissue was not permeable to primary antibodies, and therefore that Rst staining was not an artifact caused by compromised tissue integrity (Supplemental Figure S6). After the 3 h 45-min chase, there was very little antibody-labeled Rst remaining at the apical surface in WT retinas, indicating that the pool of Rst labeled at the apical surface had largely been endocytosed (Figure 7, I and I'). The amount of intracellular Rst was noticeably reduced in WT retinas after the longer chase (Figure 7, Q, Q', S, S', and U; 18% as many puncta per ommatidium; n = 104 ommatidia; p < 1 × 10⁻¹⁵). In contrast, although antibody-labeled Rst was similarly depleted from the apical surface in *Sac1ts* retinas after 3 h 45 min (Figure 7, J and J'), there was much greater persistence of bright Rst-positive puncta in 2°/3°pc relative to after 45 min than in WT (Figure 7, R, R', T, and T'). Indeed, there were 70% as many puncta per ommatidium in *Sac1ts* after the 3 h 45-min chase as in *Sac1ts* after the 45-min chase (Figure 7U; n = 104 ommatidia; p < 1 × 10⁻⁹). Thus, although internalization of antibody-labeled Rst from the PM was not impaired in *Sac1ts* retinas, degradation of the internalized Rst was delayed. Loss of Sac1 therefore impairs endosomal pathway function, leading to IRM protein accumulation within the timeframe of 24–42 h APF as these proteins are removed from the apical PM.

Sac1ts 2°/3°pc contain enlarged Rab7 and F–actin-positive organelles at 42 h APF

To visually assess how loss of Sac1 affects regulation of the endo-lysosomal pathway, we examined the morphology of late
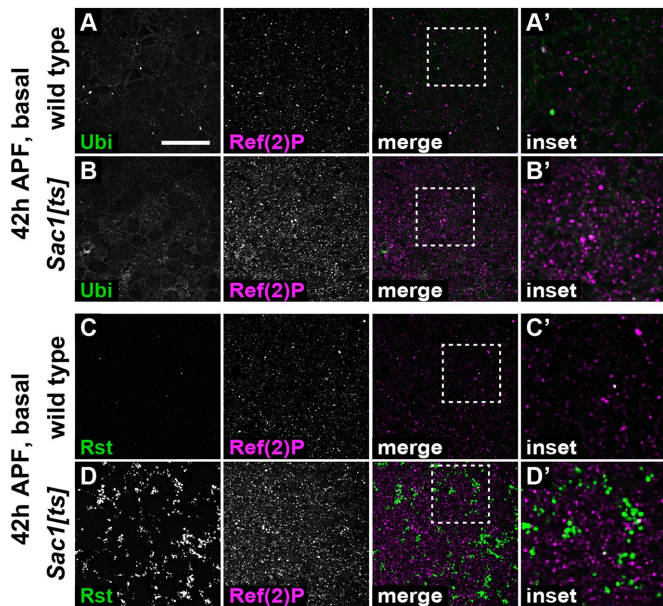
FIGURE 5: Rst is not a target of Ref(2)P-mediated autophagy in *Sac1ᵗˢ* 2°/3°pc. (A–B') Basal confocal sections of WT and *Sac1ᵗˢ* retinas at 42 h APF stained for mono- and poly-ubiquitin (Ubi, green) and Ref(2)P (magenta). (C–D') Basal confocal sections of WT and *Sac1ᵗˢ* retinas at 42 h APF stained for Rst (green) and Ref(2)P (magenta). Boxed regions in A–D are magnified 2.5-fold in A'–D'. Although Ref(2)P is more abundant in *Sac1ᵗˢ*, it does not label Rst puncta. White in merged images indicates colocalization. Scale bar: 15 μm.

endosomes and lysosomes in *Sac1ᵗˢ* retinas. Notably, *Sac1ᵗˢ* 2°/3°pc contained enlarged, basal Rab7-positive organelles that were absent in WT retinas (Figure 8, A–B'). These organelles were not Arl8-positive and thus constitute late endosomes that have not matured to the point of fusion with lysosomes. However, they frequently stained positive for F-actin (Figure 8, B, B', D, and D'). We did not observe these structures at 24 h APF, indicating they appear between 24 and 42 h APF (Supplemental Figure S7), or approximately the same timeframe as Rst and Kirre accumulation.

Late endosome to lysosome fusion is mediated by the multiprotein HOPS complex. To examine whether the enlarged late endosomes were endosome–lysosome fusion competent or were unable to progress to this stage, we costained *Sac1ᵗˢ* retinas for Rab7 and the HOPS subunit Vps16a at 42 h APF. As with Arl8, although there were instances of colocalization between Rab7 and Vps16a on small endosomes in both *Sac1ᵗˢ* and WT retinas, the enlarged basal Rab7-positive endosomes in *Sac1ᵗˢ* were not decorated with Vps16a (Figure 8, C–D').

To assess whether these enlarged endosomes are decorated with PI4P, the chief Sac1 substrate, we examined the localization of a PI4P biosensor that consists of mCherry fused to tandem PI4P-binding domains from the *Legionella* protein SidM (P4M) (mCh-2xP4M) (Hammond *et al.*, 2014; Ma *et al.*, 2020). In *Sac1ᵗˢ* mutant retinas, we observed a striking accumulation of mCh-2xP4M in basal (but not apical or medial) regions along cell membranes and in intracellular puncta in comparison to control retinas, which were either *Sac1ᵗˢ* heterozygotes (Figure 8, E–F'; Supplemental Figure S8) or WT (not shown; indistinguishable from *Sac1ᵗˢ* heterozygotes). This included noticeable PI4P accumulation on the enlarged F-actin and/or Rab7-positive endosomal compartments (Figure 8, F and F', yellow arrows).

We also performed LysoTracker staining to determine whether basal enlarged endosomes were acidified and whether the overall

size and distribution of acidified structures were affected in *Sac1ᵗˢ*. WT retinas contained LysoTracker-positive puncta that were uniform in size and apical-basal distribution (Figure 8, G and G'; Supplemental Figure S9, A and C). In contrast, in *Sac1ᵗˢ* retinas, LysoTracker staining revealed slightly irregular puncta apically (Supplemental Figure S9B), few puncta medially (Supplemental Figure S9D), and enlarged acidified structures basally that were marked with F-actin (Figure 8, H and H'). These structures thus appear to constitute the same pool of enlarged basal endosomes as those marked with Rab7.

Counterintuitively, when we compared the distribution of Rst to that of F-actin (Figure 9), it was clear that Rst does not accumulate within the enlarged F–actin-positive basal endosomes in *Sac1ᵗˢ* (Figure 9B"). Therefore, these endosomes either do not carry internalized proteins from the PM, do not contain Rst because it is arrested in an earlier endosomal compartment, are impermeable to antibodies, or are capable of degrading their cargo. The precise nature of the compartments in which Rst and Kirre accumulate in addition to YFP–Rab7-labeled late endosomes thus remains unclear. Nonetheless, we have demonstrated that Sac1 is required for both Rst turnover through the endo-lysosomal pathway and maintenance of normal endosome morphology.

OSBP is not required for Rst or Mys distribution at 42 h APF
Given its localization to the ER and *cis*-Golgi, how Sac1 is able to affect the endosomal pathway remains an enigma. In mammalian cells, OSBP delivers PI4P from the TGN to Sac1 in the ER, and chemical inhibition or knockdown of OSBP has been shown to increase the amount of PI4P on endosomes (Loewen *et al.*, 2003; Dong *et al.*, 2016; Mesmin *et al.*, 2017). Hence, we were curious whether Sac1's ability to regulate the endosomal pathway in the *Drosophila* retina depends on OSBP. Interestingly, loss of OSBP did not result in the dramatic accumulation of Rst that we observed in *Sac1ᵗˢ* retinas. In null *osbp* mutants, the number of Rst puncta per ommatidium was modestly increased compared with WT in basal sections (Figure 10, A–C; $n = 48$ ommatidia, $p < 1 \times 10^{-10}$) as well as medial sections (Figure 10C; $n = 48$ ommatidia, $p < 1 \times 10^{-5}$) at 48 h APF, which, due to a slight developmental delay, is approximately the equivalent stage to 42 h APF in WT and *Sac1ᵗˢ* retinas (44% of pupal development; p44%). However, this was very mild compared with the dramatic phenotype in *Sac1ᵗˢ* retinas at 42 h APF (Figure 2, F and F'). We also observed some scattered instances of enlarged basal F-actin compartments in *osbp* retinas (Figure 10, B, B', E and E', yellow arrows), but less consistently and in much lower abundance than in *Sac1ᵗˢ*. Similarly, whereas Mys localization at the basal grommets was disrupted in *Sac1ᵗˢ*, in *osbp* retinas both basal patterning and Mys distribution appeared unperturbed at p44% (Figure 10, D–E'). Therefore, OSBP is not strictly required for Sac1 function in the developing *Drosophila* eye. Precisely how Sac1 oversees endosomal regulation and protein turnover in the fly, including the routes of lipid transport involved, is an intriguing question for further study.

DISCUSSION
The *Drosophila* pupal eye represents a powerful system to examine protein trafficking and turnover. Patterning of retinal cells requires spatially and temporally regulated expression as well as correct subcellular distribution of cell surface proteins that mediate cell–cell contacts and determine tissue architecture. Dysregulation of these processes can produce structural defects, which frequently persist in the adult eye. We have taken advantage of these circumstances to demonstrate the importance of Sac1 in basal delivery of the β_ps-integrin Mys, which is required for retinal floor integrity, as well as
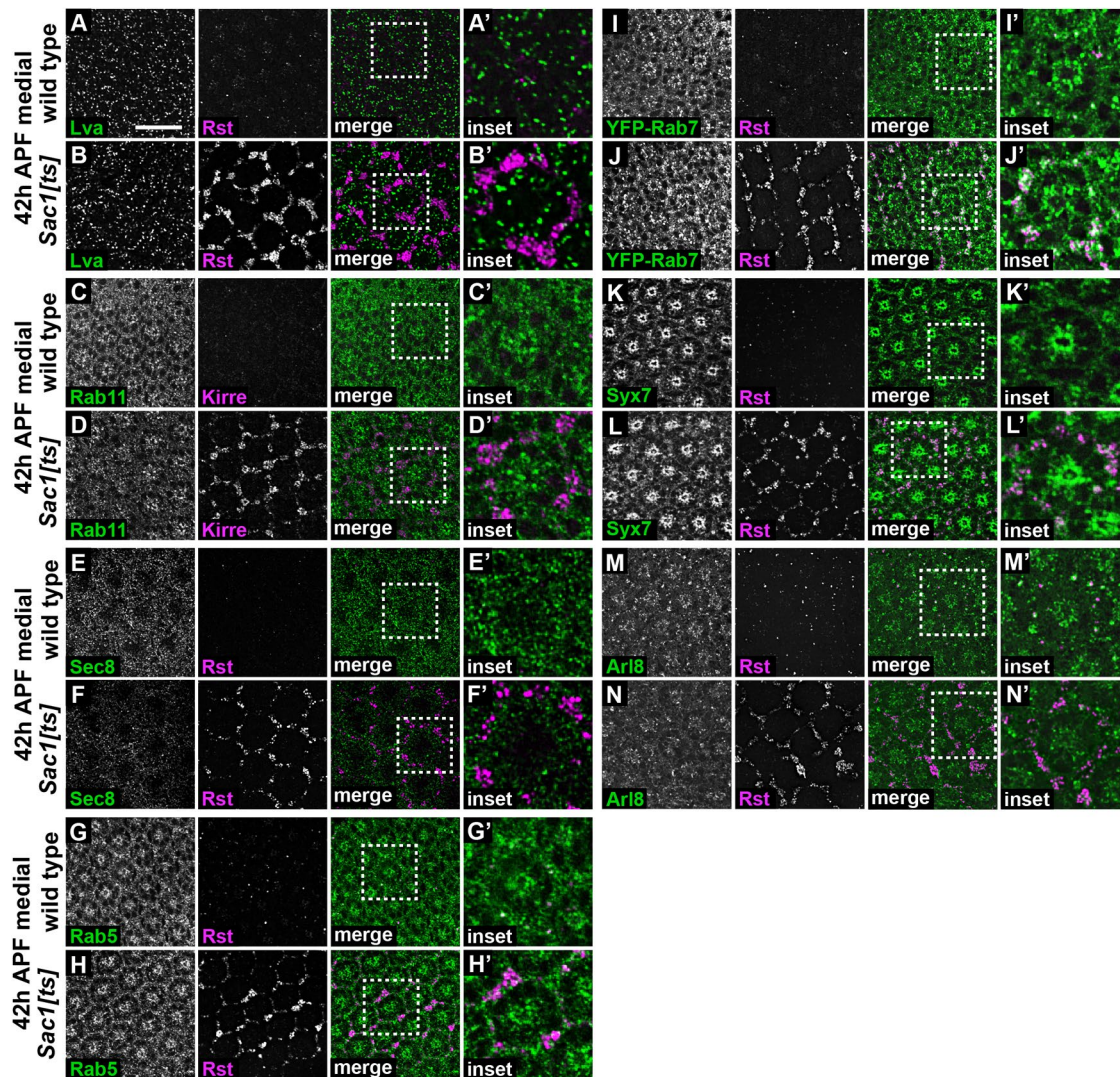
FIGURE 6: Rst colocalizes with late endosome markers in *Sac1ts* 2°/3°pc. (A–N) Medial confocal sections of 42 h APF retinas stained for Rst or Kirre (magenta) and additional proteins (green) to mark specific subcellular compartments. Boxed regions are magnified in insets (A'–N'). White in merged images indicates colocalization. In all cases, *Sac1ts* 2°/3°pc accumulate Rst/Kirre. In *Sac1ts*, Rst partially colocalizes with YFP-Rab7 (J) and to a lesser extent with Syx7 (L). Scale bar: 15 µm.

endo-lysosomal regulation and turnover of the apical patterning determinants Rst and Kirre. Our results also highlight the importance of *Drosophila* Sac1 in ER homeostasis, as had been reported in yeast (Mayinger *et al.*, 1995; Kochendorfer *et al.*, 1999). This could be due to deregulation of PI4P, phosphatidylserine, and sterol levels, which would be expected to disrupt ER membrane charge and lipid order.

Given the similarities between *mys* mutants and *Sac1ts* (Longley and Ready, 1995), loss of Mys at the basal grommets in *Sac1ts* likely causes the retinal floor defects we observed in the adult eye. In addition, this phenotype resembles the basal retinal degeneration observed in an ALS-associated *vap* mutant (Forrest *et al.*, 2013), suggesting the underlying cause could be similar. However, it is unclear why basal distribution of Mys is perturbed while apical polarity is not. In the *Drosophila* follicular epithelium, Rab10 activity has been shown to be important for the distribution of basement membrane proteins independent of overall apical-basal polarity, in a manner dependent on PI(4,5)P$_2$ at the apical PM (Devergne *et al.*, 2014). We previously observed a decrease in apical PI(4,5)P$_2$ abundance in

Sac1ts retinas at 24 h APF (Del Bel *et al.*, 2018), which we speculate could perturb basal trafficking. Alternatively, aberrant distribution of basal F-actin in *Sac1ts* could inhibit localization of Mys to the grommets. Why some transmembrane proteins are sensitive to reduced Sac1 activity while others are not remains an open question. It is also unclear whether Mys mislocalization is linked to endosome dysfunction in *Sac1ts*.

Whereas PI3P and PI(3,5)P$_2$ are the canonical phosphoinositide regulators of endosomal progression (Wallroth and Haucke, 2018), PI4P production has also emerged as an important factor in cargo delivery to lysosomes. In mammalian cells, PI4P is generated on late endosomes by type II PI4Ks (Baba *et al.*, 2019). PI4KIIα is important for Golgi-to-lysosome trafficking of LIMP-2, as well as PM-to-lysosome trafficking of LAMP-1, and these proteins accumulate in enlarged endosomes when PI4KIIα levels are reduced (Craige *et al.*, 2008; Jovic *et al.*, 2012). Furthermore, in macrophages, PI4KIIα-mediated PI4P enrichment on phagosomes occurs concurrently with Rab7 recruitment and is necessary for phagosome acidification and subsequent fusion with lysosomes (Levin *et al.*, 2017).
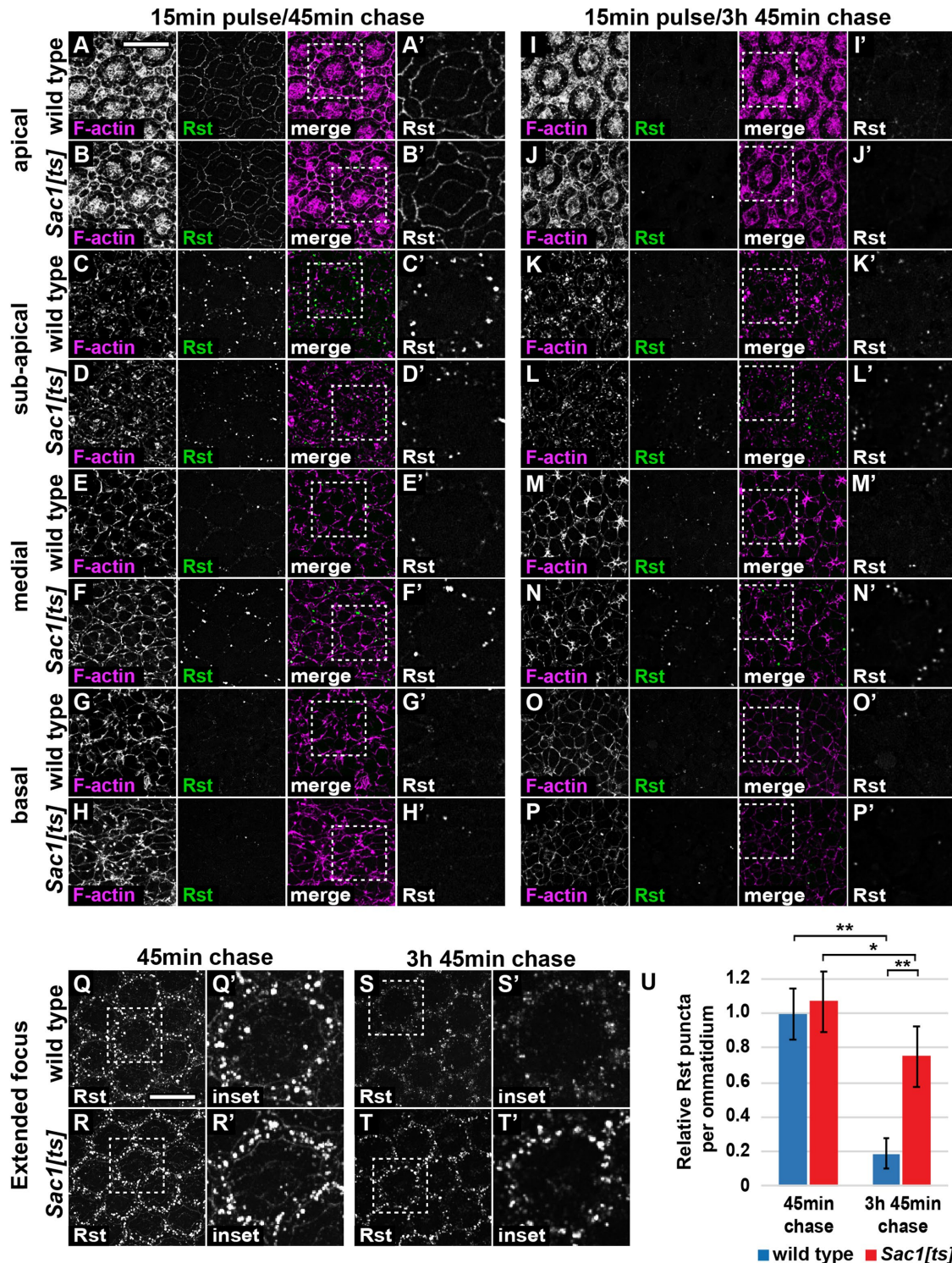
FIGURE 7: Endosomal trafficking and degradation of antibody-labeled Rst is delayed in *Sac1[ts]*. (A–P') Confocal sections of WT and *Sac1[ts]* retinas stained for F-actin (phalloidin, magenta) and Rst (green). (A–H') Retinas were dissected at 28 h APF, incubated with anti-Rst antibodies for 15 min at 25°C, washed, cultured in growth medium with serum for an additional 45 min at 25°C, then washed, fixed, permeabilized, and stained with fluorescently conjugated secondary antibodies. (I–P') Retinas were treated as in A–H' but were cultured for 3 h 45 min prior to fixation. Boxed regions in A–P are magnified twofold in A'–P'. (Q–T') Extended projections spanning the apical to basal surface of WT and *Sac1[ts]* retinas stained for Rst depicted in A–P'. Z-spacing: 0.3 µm. Boxed regions in Q–T are magnified threefold in Q'–T'. (U) Number of Rst puncta per ommatidium relative to WT after a 45-min or 3 h 45-min chase. Puncta were defined by minimum size and intensity. *Sac1[ts]* after 45 min had 107% as many Rst puncta as WT after 45 min; *Sac1[ts]* after 3 h 45 min had 76% as many Rst puncta as WT after 45 min. Error bars represent SD; $n = 104$ ommatidia from a total of 26 eyes from three independent experiments. $*p < 1 \times 10^{-9}$, $**p < 1 \times 10^{-15}$, two-tailed Student's *t* test. Scale bars: 15 µm.
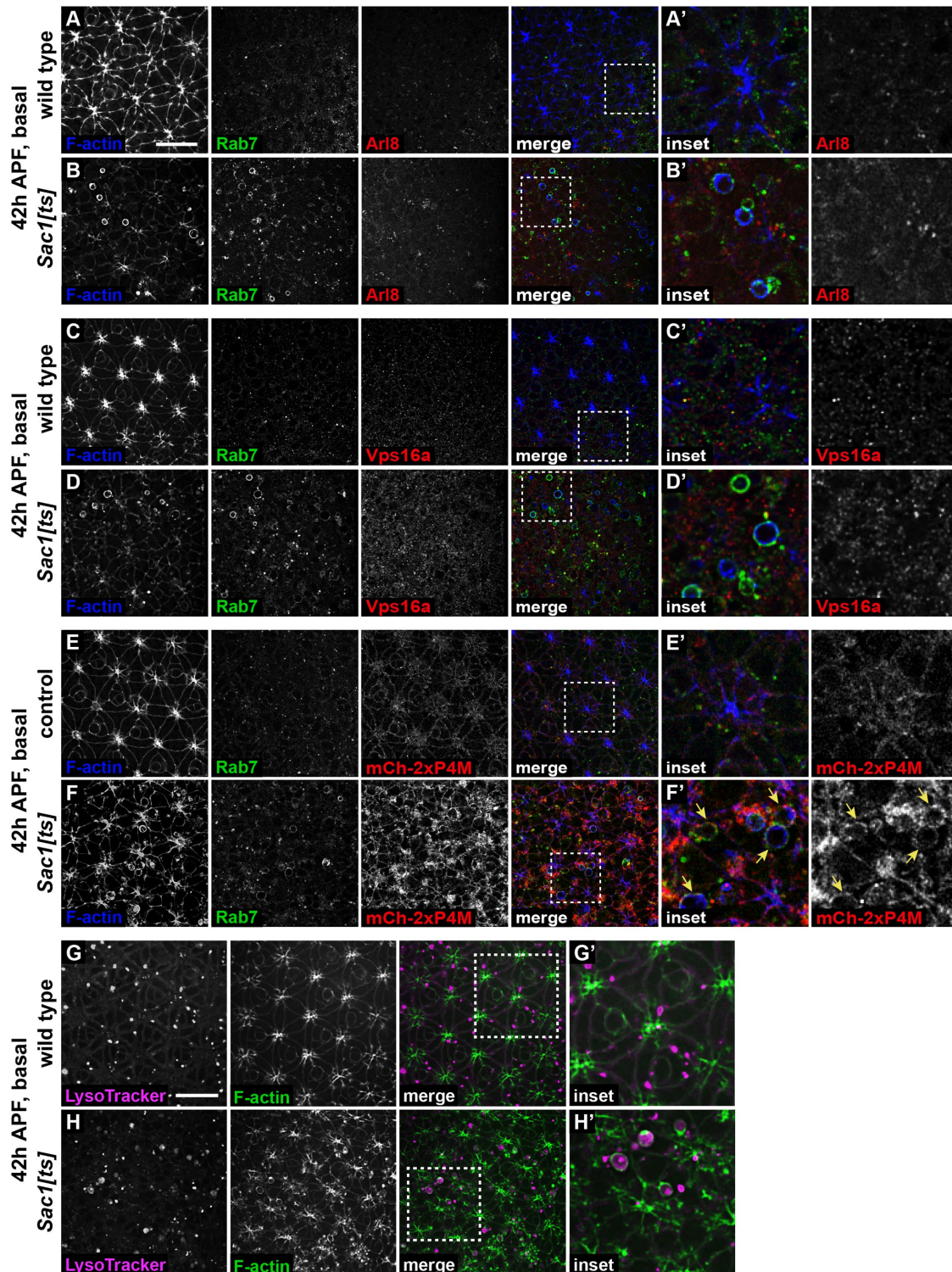
FIGURE 8: *Sac1ᵗˢ* 2°/3°pc contain F–actin-positive enlarged late endosomes. (A–D') Basal confocal sections of WT and *Sac1ᵗˢ* retinas at 42 h APF stained for F-actin (phalloidin, blue), Rab7 (green), and either Arl8 (red, A–B') or Vps16a (red, C–D'). (E–F') Basal confocal sections of *Sac1ᵗˢ* homozygous or heterozygous (control) retinas expressing mCh-2xP4M at 42 h APF, stained for F-actin (phalloidin, blue), Rab7 (green), and mCherry (red). Boxed regions in A–F are magnified threefold in A'–F'. Arrows in F' indicate enlarged Rab7-positive endosomes that are also mCh-2xP4M-positive. Yellow in merged images indicates colocalization between green and red. (G–H') Basal confocal sections of WT and *Sac1ᵗˢ* retinas at 42 h APF stained with LysoTracker (magenta, to mark acidified organelles) and F-actin (phalloidin, green). Boxed regions in G and H are magnified twofold in G' and H'. *Sac1ᵗˢ* retinas contain acidified enlarged F–actin-positive endosomes that are likely labeled with both Rab7 and mCh-2xP4M but not Arl8 or Vps16a. Scale bars: 15 μm.
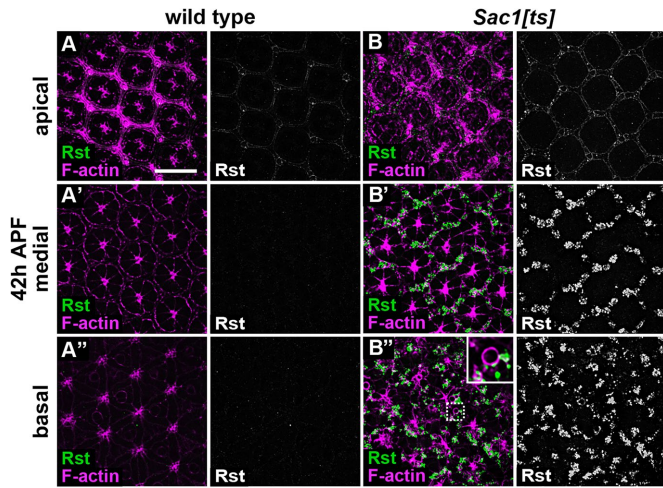
FIGURE 9: Rst does not accumulate in enlarged basal F–actin-positive endosomes. (A–B") Confocal sections of WT and *Sac1[ts]* retinas at 42 h APF, stained for Rst (green) and F-actin (phalloidin, magenta). Rst accumulation is apparent in medial and basal regions of *Sac1[ts]* 2°/3°pc (B' and B"). Cell borders are highlighted by cortical F-actin. Rst is excluded from enlarged basal F–actin-positive compartments in *Sac1[ts]* 2°/3°pc (B"). Boxed inset in B" is magnified threefold. Scale bar: 15 µm.

Here, we have shown that Sac1-dependent depletion of PI4P is also important for endosomal trafficking and degradation of transmembrane proteins from the PM. This is consistent with a recent report by Mao and colleagues (Mao *et al.*, 2019), who found that in multiple larval *Drosophila* tissues, loss of VAP, which recruits OSBP and a subset of ORPs to MCS, increases endosomal PI4P levels and inhibits autophagic degradation. Null *vap* mutants exhibit decreased lysosomal acidification, as well as an increase in the abundance of lysosomes, endosomes, autolysosomes, autophagosomes, and Ref(2)P (Mao *et al.*, 2019). The authors propose that increased PI4P abundance up-regulates endosome formation and progression, which causes lysosomes to become oversaturated with incoming cargo. Indeed, loss of Ubiquilin, which contributes to lysosome acidification, also delays autophagy and causes Ref(2)P buildup (Şentürk *et al.*, 2019). Notably, we observed increased Ref(2)P abundance in *Sac1[ts]* retinas, which suggests a similar delay in autophagy. It is a compelling notion that increased PI4P levels in *Sac1[ts]* could promote excessive fusion of endosomes with lysosomes, which would replicate the effect described by Mao and colleagues (2019). However, the accumulation of Rst and Kirre in *Sac1[ts]*, which do not appear to be concentrated in lysosomes based on the lack of colocalization between Rst and Arl8, could also be caused by impaired endosomal progression or maturation, though this might stem from downstream lysosomal dysfunction. Indeed, the enlarged endosomes we observed in *Sac1[ts]* lacked both Vps16a and Arl8, suggesting they were
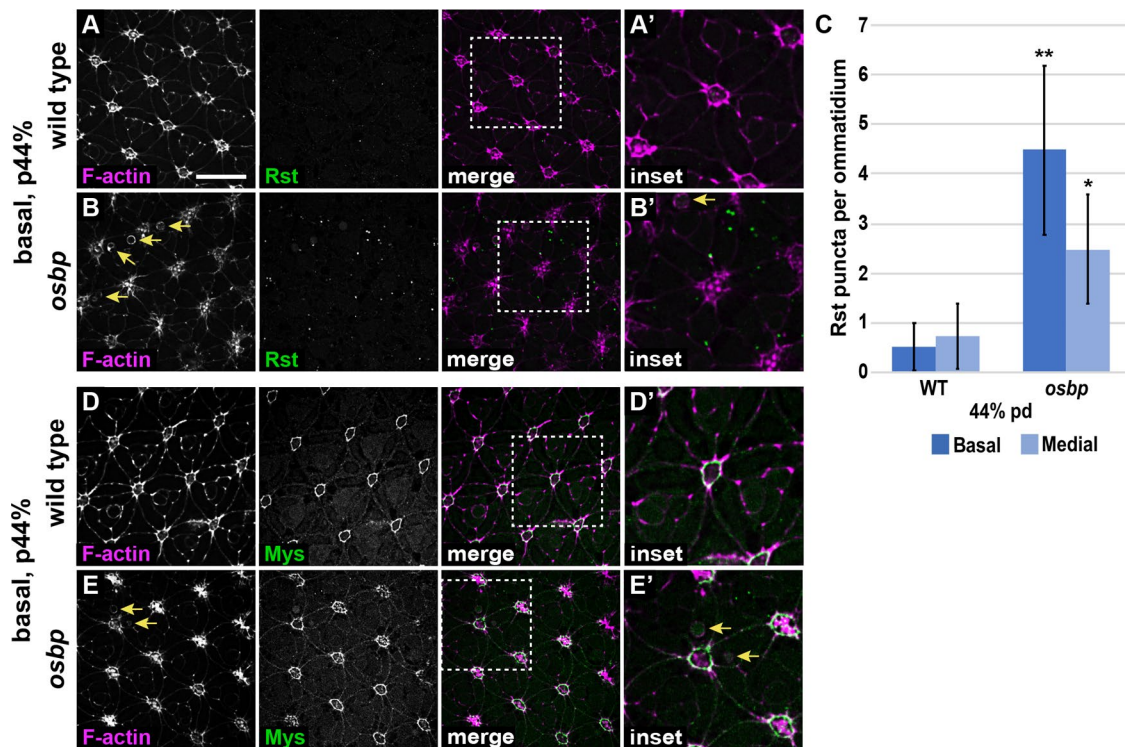
FIGURE 10: *osbp* retinas display normal basal patterning and mild Rst accumulation. (A–B') Basal confocal sections of WT and *osbp* retinas at 42 h APF and 48 h APF, respectively (p44%), stained for F-actin (phalloidin, magenta) and Rst (green). Boxed regions in A and B are magnified twofold in A' and B'. Yellow arrows indicate enlarged F–actin-positive compartments. (C) Quantification of the number of Rst puncta in medial and basal sections per ommatidium. Puncta were defined by minimum size and intensity. Error bars represent SD; *n* = 48 ommatidia from a total of 16 eyes from three independent experiments. *$p < 1 \times 10^{-5}$, **$p < 1 \times 10^{-10}$, two-tailed Student's *t* test. (D–E') Basal confocal sections of WT and *osbp* retinas at 42 h APF and 48 h APF, respectively (p44%), stained for F-actin (phalloidin, magenta) and Mys (green). Boxed regions in D and E are magnified twofold in D' and E'. White in merged images indicates colocalization. Scale bar: 15 µm.

not caused by excessive fusion with lysosomes. Further analysis of PI4P in endosomal dynamics and maturation is warranted to determine the precise role of Sac1 in late stages of protein degradation.

We also found that reduced Sac1 function leads to basal accumulation of F–actin-positive enlarged endosomes. In mammalian cells, loss of both VAP isoforms has been shown to induce F-actin comet formation on endosomes via PI4P-dependent recruitment of the WASH-ARP2/3 complex (Dong *et al.*, 2016). Notably, these do not resemble the more uniform F-actin coating on *Sac1ts* endosomes. Rather, the structures we observed appear more reminiscent of a phenomenon termed actin-flashing, wherein phagosomes become coated in F-actin by WASP-ARP2/3 to delay fusion with lysosomes (Liebl and Griffiths, 2009; Johnston and May, 2010). Endosomal phenotypes similar to those in *Sac1ts* have also been observed when Arf6 activity is perturbed; increased Arf6 activity activates PIP5K, which has been shown to produce PI(4,5)P_2 on endosomes and lead to F-actin polymerization via WASP (Brown *et al.*, 2001), whereas loss of Arf6 increases endosomal PI4P levels and perturbs endosomal recycling (Marquer *et al.*, 2016). Intriguingly, in *Caenorhabditis elegans,* Sac1 inhibits Arf6 by sequestering the Arf6-GEF Bris-1 (Chen *et al.*, 2018). However, it is unknown whether this interaction is conserved or, more broadly, how Sac1 influences F-actin polymerization on endosomes.

It is noteworthy that enlarged endosomes were restricted to basal regions in *Sac1ts*. Positioning of endosomes and lysosomes is mediated by bidirectional transport along microtubules, which influences their acidity and function (Johnson *et al.*, 2016). In mammalian cells, Rab7 recruits RILP, which activates endosomal dynein motors to promote minus end-directed transport toward perinuclear microtubule organizing centers (Cantalupo *et al.*, 2001; Jordens *et al.*, 2001; Johansson *et al.*, 2007; Wijdeven *et al.*, 2016). PI4P is also required for RILP recruitment (Levin *et al.*, 2017), which implies that excess PI4P could lead to perinuclear endosome accumulation. Although the single *Drosophila* RILP orthologue has been shown to bind Arl8 rather than Rab7 (Rosa-Ferreira *et al.*, 2018), it is possible that PI4P influences late endosome transport through analogous Rab7 effectors. Additionally, we previously showed that *Sac1ts* 2°/3°pc precursors contain unstable microtubules at 24 h APF (Del Bel *et al.*, 2018), which could affect microtubule-based endosome positioning later in development (although we were unable to detect microtubule defects by immunostaining at 42 h APF; not shown). However, it is also possible that enlarged endosomes accumulate basally for other reasons or are simply excluded from narrower apical-medial regions on the basis of size. It remains to be discerned whether Rst accumulation and the appearance of enlarged endosomes, which co-occurred between 24 and 42 h APF, share a causal basis or represent distinct, parallel phenotypes of reduced Sac1 activity.

Given the phenotypic similarities between *Sac1ts* and *vap* mutants (Mao *et al.*, 2019), it was surprising that *osbp* did not affect Mys distribution or cause severe Rst accumulation. However, this is reminiscent of previous results from *Drosophila* neurons, where loss of Vap but not OSBP caused protein accumulation and ER stress (Moustaqim-Barrette *et al.*, 2014). It is possible that, as in yeast where the presence of one out of seven OSBP homologues is sufficient for viability, OSBP functions redundantly with one or more ORPs in regulating the endosomal pathway. Indeed, *CG1513*, which is synthetically lethal in combination with *osbp* (Moustaqim-Barrette *et al.*, 2014), encodes an orthologue of mammalian ORP9, which functions similarly to OSBP in sterol–PI4P exchange at ER–Golgi MCS (Liu and Ridgway, 2014; Venditti *et al.*, 2019b). Alternatively, *CG3860* encodes an orthologue of mammalian ORP2, which localizes to late endosomes in HeLa cells and influences sterol levels in endosomes and the PM,

although countertransport of PI4P has not been shown (Koponen *et al.*, 2018; Wang *et al.*, 2019). Mammalian ORP2 also binds ORP1L (Koponen *et al.*, 2018), which acts at ER–endosome MCS and promotes endosome transport, though it is unclear whether such a role is conserved in *Drosophila,* which lack an ORP1L orthologue (Rocha *et al.*, 2009; Vihervaara *et al.*, 2011; van der Kant *et al.*, 2013; Wijdeven *et al.*, 2016; Zhao and Ridgway, 2017). Further characterization of the *Drosophila* ORPs is thus needed to clarify their respective contributions to lipid homeostasis and endosomal progression.

Recent years have seen a proliferation of research into Sac1's roles in lipid homeostasis and the importance of PI4P regulation, as well as the development of novel probes and methods for studying phosphoinositides in vivo. We have provided new insights into Sac1's function in protein delivery and turnover in a developing tissue, which we hope will serve as groundwork for further investigations into the significance of Sac1 in cell physiology, organismal development, and ultimately cellular homeostasis in human health and disease.

MATERIALS AND METHODS

Fly stocks
Flies were raised on standard cornmeal molasses agar (Ashburner, 1990). Crosses and staging were performed at 25°C, unless otherwise specified. WT and *Sac1ts* flies used were Oregon R (WT) and *w⁺; Sac1ts* or *w⁺; Sco/CyO; FRT80B, Sac1ts* (*Sac1ts*) (Wei *et al.*, 2003b; Del Bel *et al.*, 2018). The following rescue constructs on chromosome II were crossed into the *Sac1ts* mutant background: P{*w⁺*, α_1-tubulin>mCherry-Sac1(WT)} (WT Sac1) and P{*w⁺*, α_1-tubulin>mCherry-Sac1(PR)} (PR Sac1) (Del Bel *et al.*, 2018). Additional stocks were P{*w⁺*, α_1-tubulin>YFP-Rab7/CyO} (from the late S. Eaton, Dresden, Germany) (Marois *et al.*, 2006), *w; UAS- xbp1-EGFP, tub-Gal4/CyO* (from H. D. Ryoo, New York) (Sone *et al.*, 2013), *hsflp;; FRT80B, GFP* (Bloomington Drosophila Stock Center), *w; αTub84B>mCh-2xP4M; Sac1ts* or *w; αTub84B>mCh-2xP4M; Sac1ts/TM6B*) (from C-I. J. Ma and G. Polevoy, Toronto, Canada) (Ma *et al.*, 2020), and *w; Sco/CyO; osbp¹* (from X. Huang, Beijing, China) (Ma *et al.*, 2010).

Generation of *Sac1ts* mutant clones
Sac1ts mutant clones were generated by FRT-mediated recombination (Xu and Rubin, 1993) using flies of the following genotype: *hsflp;; FRT80B, GFP/ FRT80B, Sac1ts*. Clones were induced by heat-shocking larvae 72 h after egg laying for 1 h at 37°C. Clones are homozygous mutant for *Sac1ts* and GFP-negative.

Thick sections and light microscopy
Eyes from 3-d-old male flies raised at 23.5°C were sectioned and examined by light microscopy. Note that this temperature was chosen to ensure that enough flies survived to adulthood for the analysis. Eyes were dissected, fixed, embedded in Durcopan resin, baked, and sectioned as described (Wolff, 2000), with the following exceptions: 1% osmium was used instead of 2% and samples were not stained with toluidine blue. Samples were sectioned at the Advanced Bioimaging Center at Mount Sinai Hospital, Toronto, Canada. Light micrographs of thick (1 μm) sections were acquired with a Zeiss Axiocam CCD camera on an Axioplan 2E microscope equipped with phase-contrast 100× Zeiss objectives using Zeiss Axiovision software. Images were exported and uniformly manipulated for brightness and contrast using Photoshop CS6.

Measuring ommatidial length
Average ommatidial length was determined using the Line tool in Volocity 3D Image Analysis Software 6.3.1 (PerkinElmer) (SickKids Imaging Facility, Toronto, Canada). Statistical analysis

was performed with the Student's *t* test using values normalized to WT.

TEM

Fly eyes were prepared for TEM as described (Pellikka *et al.*, 2002). In brief, heads from 3-d-old flies were immobilized in phosphate-buffered saline (PBS), bisected, and fixed in 1% OsO_4 in 0.1 M Cacodylate buffer. Samples were left in fixative for 3 d on a nutator at 4°C. Samples were then washed with 0.1 M Cacodylate buffer, placed in fixative in the dark for 1 h, washed again with 0.1 M Cacodylate buffer, and dehydrated in an ethanol series (50, 70, 80, 90, and 100% for 5 min each). Next, samples were embedded in fresh Spurr's resin and polymerized in rubber molds at 65°C for 8 h. Finally, embedded samples were sectioned (Reichert Ultracut E ultramicrotome) and imaged using a FEI Tecnai 20 transmission electron microscope (Advanced Bioimaging Center, Mount Sinai Hospital, Toronto, Canada). Images were uniformly edited with Adobe Photoshop CS6.

Immunocytochemistry

Pupal retinas were dissected in PBS as described by Walther and Pichaud (2006), fixed in 4% paraformaldehyde (PFA) for 30 min, then washed in PBS. Fixation was performed either on ice (Figures 2–4 and 6; and Supplemental Figures S1, S2, S4, and 8) or at room temperature (RT) (Figures 1, 5, 8, A–F', 9, and 10; and Supplemental Figures S3 and S5–S7). For stainings that were performed with both fixation temperatures, we obtained similar results (e.g., Rst in Figures 2 and 9). After fixation, samples were permeabilized by washing with PBS + 0.3% saponin (PBSS) for 10 min, blocked with 5% normal goat serum (NGS) (Invitrogen, 31873) in PBSS for 1 h at RT, then incubated with primary antibodies in PBSS with 5% NGS overnight at 4°C, washed in PBSS, and incubated with secondary antibodies with rhodamine or Alexa Fluor 633–conjugated phalloidin (4 U/ml) (Thermo Fisher, R415, A22284) in PBSS with 10% NGS for 2–4 h at RT in the dark. After secondary antibody staining, samples were washed in PBSS, detached from optic lobes, and mounted on Thermo Fisher Polysine slides using Dako Fluorescence Mounting Media (Agilent, S3023) or ProLong Diamond Antifade Mountant (Thermo Fisher, P36970). DAPI (Thermo Fisher, D1306) was prepared at 1:1000 in PBSS and applied for 10 min at RT in the dark after secondary antibody staining.

Primary antibodies were mouse anti-Rst mAb24A5.1 (from K. F. Fischbach, Freiburg, Germany, 1:50) (Schneider *et al.*, 1995), rabbit anti-Kirre (from K. F. Fischbach, 1:300), mouse anti-Notch[ECD] C458.2H (Developmental Studies Hybridoma Bank [DSHB], 1:200) (Diederich *et al.*, 1994), mouse-anti Notch[ICD] C17.9C6 (DSHB, 1:500) (Fehon *et al.*, 1990), mouse anti-Mys CF.6G11 (DSHB, 1:100) (Brower *et al.*, 1984), mouse anti-Arm N2 7A1 (DSHB, 1:150) (Riggleman *et al.*, 1990), rat anti-DE-Cad DCAD2 (DSHB, 1:50) (Oda *et al.*, 1994), mouse anti-Dlg 4F3 (DSHB,1:500) (Parnas *et al.*, 2001), rabbit anti-BiP/GRP78 (StressMarq Biosciences SPC-180D, 1:100), mouse anti-GFP 3E6 (Life Technologies/Invitrogen, A111-20, 1:500), chicken anti-GFP (AbCam13970, 1:500), mouse anti-KDEL (Enzo Stressgen SPA-827, 1:250), guinea pig anti-Sec8 (from U. Tepass, Toronto, Canada, 1:1000) (Beronja *et al.*, 2005), mouse anti-Lva (from the late J. Sisson and O. Papoulas, Austin, TX, 1:1000) (Sisson *et al.*, 2000), rabbit anti-Rab5 (from M. Gonzales-Gaitan, Dresden, Germany, 1:50) (Wucherpfennig *et al.*, 2003), mouse anti-Rab11 (BD Bioscience, 1:50), rabbit anti-Syntaxin7 (from H. Krämer, Dallas, TX, 1:1000), mouse anti-Rab7 (DSHB, 1:15) (Riedel *et al.*, 2016), rabbit anti-Arl8 (from S. Munro, Cambridge, UK, 1:1000 or DSHB, 1:200) (Hofmann and Munro, 2006), rabbit anti-Vps16a (from H. Krämer,

Dallas, TX, 1:200) (Pulipparacharuvil *et al.*, 2005), rabbit anti-Ref(2)P (from T. E. Rusten, Oslo, Norway, 1:1000) (Nezis *et al.*, 2008), mouse anti-mono/polyubiquitin FK2 (Enzo Life Sciences, 1:100), and rat anti-RFP 5F8 (Chromotek, 1:500). Secondary antibodies conjugated to Alexa Fluor 488, 568, and 633 (Thermo Fisher) were used at 1:500.

To stain acidified structures, pupal eyes were dissected in PBS and incubated for 20 min at RT with LysoTracker Red at 1:1000 (Thermo Fisher). Samples were then washed with PBS, fixed in 4% PFA for 30 min on ice, washed again, permeabilized with PBSS, stained with phalloidin as described above, and mounted for imaging.

Dithiothreitol (DTT) treatments

Eye–brain complexes from OreR and *w; UAS- xbp1-EGFP, tub-Gal4/ CyO* pupae were dissected at 28 h in Schneider's medium containing 10% fetal bovine serum (10% FBS) and cultured for 4 h at RT with gentle shaking in Schneider's medium (10% FBS) containing DTT. After DTT treatment, samples were washed in PBS, then fixed and stained as described above.

Antibody uptake and degradation assay

Pupal eye–brain complexes were dissected in Schneider's medium (10% FBS), incubated in anti-Rst (1:50) and anti-Lva (1:500) in Schneider's medium (10% FBS) and 10% NGS for 15 min at 25°C (pulse), washed, and incubated in Schneider's medium (10% FBS) at 25°C with gentle shaking for either 45 min or 3 h 45 min (chase). During ex vivo culture for antibody pulse/chase, eyes were used that remained attached to intact brains. Samples were washed in PBS and fixed in 4% PFA for 30 min at RT, permeabilized by washing in PBSS, blocked in 10% NGS for 1 h at RT, incubated with secondary antibodies and rhodamine phalloidin (4 U/ml) (Thermo Fisher, R415) in PBSS with 10% NGS for 2–4 h at RT in the dark, and washed in PBSS. Eyes were detached from optic lobes and mounted in ProLong Diamond Antifade Mountant (Thermo Fisher, P36970).

Confocal imaging and analysis

Images were acquired using a Quorum spinning disk confocal microscope with the following components: Olympus IX81 inverted microscope; Yokogawa CSU-X1 scanhead; 60×/1.35NA oil-immersion objective, Improvision Piezo focus drive; Spectral Borealis 405-, 491-, 561-, and 642-nm lasers (50 mW); Hamamatsu C9100-13 EM-CCD camera; and Perkin Elmer Volocity 6.3 software (SickKids Imaging Facility, Toronto, Canada). Serial optical sections were obtained with a z-spacing of 0.3 μm. For figure preparation, z-stacks were deconvolved using the Iterative Restoration function in Volocity. Images were exported, and brightness and contrast were uniformly adjusted using Adobe Photoshop CS6 and Creative Cloud. Boxed insets in Figures 1, I and L, and 9B" were resampled to 300 pixels per inch after enlargement.

Quantification of Rst puncta per ommatidium was done using the Volocity Measurements tool. Puncta were defined as a minimum number of adjacent pixels above a threshold intensity. Ommatidia were defined using a round region of interest (ROI). For Rst antibody uptake at 24 h APF and comparison of Rst puncta in *osbp* and WT, puncta were measured in single equivalent planes. For Rst antibody uptake and degradation at 28 h APF, puncta were measured in z-stacks of serial optical sections spanning the apical-basal surfaces; ommatidia were defined using round ROIs drawn at the apical surface and applied to each section. All measurements were taken from nonneighboring ommatida using raw, unprocessed images. Statistical analysis of apical Rst intensity and number of Rst puncta

was done with the Student's *t* test using values normalized to WT. All experiments were performed three independent times.

REFERENCES
Araki K, Nagata K (2011). Protein folding and quality control in the ER. Cold Spring Harb Perspect Biol 3, a007526.

Araujo H, Machado LCH, Octacílio-Silva S, Mizutani CM, Silva MJF, Ramos RGP (2003). Requirement of the roughest gene for differentiation and time of death of interommatidial cells during pupal stages of *Drosophila* compound eye development. Mech Dev 120, 537–547.

Artero RD, Castanon I, Baylies MK (2001). The immunoglobulin-like protein Hibris functions as a dose-dependent regulator of myoblast fusion and is differentially controlled by Ras and Notch signaling. Development 128, 4251–4264.

Ashburner M (1990). *Drosophila*: A Laboratory Handbook. Cold Spring Harbor, NY: Cold Spring Harbor Press.

Baba T, Toth DJ, Sengupta N, Kim YJ, Balla T (2019). Phosphatidylinositol 4,5-bisphosphate controls Rab7 and PLEKMH1 membrane cycling during autophagosome–lysosome fusion. EMBO J 38, e100312.

Baird D, Stefan C, Audhya A, Weys S, Emr SD (2008). Assembly of the PtdIns 4-kinase Stt4 complex at the plasma membrane requires Ypp1 and Efr3. J Cell Biol 183, 1061–1074.

Balla T (2013). Phosphoinositides: Tiny lipids with giant impact on cell regulation. Physiol Rev 93, 1019–1137.

Balla A, Tuymetova G, Barshishat M, Geiszt M, Balla T (2002). Characterization of type II phosphatidylinositol 4-kinase isoforms reveals association of the enzymes with endosomal vesicular compartments. J Biol Chem 277, 20041–20050.

Balla A, Tuymetova G, Tsiomenko A, Varnai P, Balla T (2005). A plasma membrane pool of phosphatidylinositol 4-phosphate is generated by phosphatidylinositol 4-kinase type-III alpha: Studies with the PH domains of the oxysterol binding protein and FAPP1. Mol Biol Cell 16, 1282–1295.

Bao S, Cagan R (2005). Preferential adhesion mediated by Hibris and Roughest regulates morphogenesis and patterning in the *Drosophila* eye. Dev Cell 8, 925–935.

Bao S, Fischbach KF, Corbin V, Cagan RL (2010). Preferential adhesion maintains separation of ommatidia in the *Drosophila* eye. Dev Biol 344, 948–956.

Beronja S, Laprise P, Papoulas O, Pellikka M, Sisson J, Tepass U (2005). Essential function of *Drosophila* Sec6 in apical exocytosis of epithelial photoreceptor cells. J Cell Biol 169, 635–646.

Bjørkøy G, Lamark T, Brech A, Outzen H, Perander M, Øvervatn A, Stenmark H, Johansen T (2005). p62/SQSTM1 forms protein aggregates degraded by autophagy and has a protective effect on huntingtin-induced cell death. J Cell Biol 171, 603–614.

Blagoveshchenskaya A, Fei YC, Rohde HM, Glover G, Knödler A, Nicolson T, Boehmelt G, Mayinger P (2008). Integration of Golgi trafficking and growth factor signaling by the lipid phosphatase SAC1. J Cell Biol 180, 803–812.

Bour BA, Chakravarti M, West JM, Abmayr SM (2000). *Drosophila* SNS, a member of the immunoglobulin superfamily that is essential for myoblast fusion. Genes Dev 14, 1498–1511.

Brill JA, Hime GR, Scharer-Schuksz M, Fuller MT (2000). A phospholipid kinase regulates actin organization and intercellular bridge formation during germline cytokinesis. Development 127, 3855–3864.

Brower DL, Wilcox M, Piovant M, Smith RJ, Reger LA (1984). Related cell-surface antigens expressed with positional specificity in *Drosophila* imaginal discs. Proc Natl Acad Sci 81, 7485–7489.

Brown FD, Rozelle AL, Yin HL, Balla T, Donaldson JG (2001). Phosphatidylinositol 4,5-bisphosphate and Arf6-regulated membrane traffic. J Cell Biol 154, 1007–1017.

Burgess J, Del Bel LM, Ma C-IJ, Barylko B, Polevoy G, Rollins J, Albanesi JP, Kramer H, Brill JA (2012). Type II phosphatidylinositol 4-kinase regulates trafficking of secretory granule proteins in *Drosophila*. Development 139, 3040–3050.

Cagan RL, Ready DF (1989). The emergence of order in the *Drosophila* pupal retina. Dev Biol 136, 346–362.

Cantalupo G, Alifano P, Roberti V, Bruni CB, Bucci C (2001). Rab-interacting lysosomal protein (RILP): the Rab7 effector required for transport to lysosomes. EMBO J 20, 683–693.

Charman M, Goto A, Ridgway ND (2017). Oxysterol-binding protein recruitment and activity at the endoplasmic reticulum-Golgi interface are independent of Sac1. Traffic 18, 519–529.

Chen D, Yang C, Liu S, Hang W, Wang X, Chen J, Shi A (2018). SAC-1 ensures epithelial endocytic recycling by restricting ARF-6 activity. J Cell Biol 217, 1–27.

Chung J, Torta F, Masai K, Lucast L, Czapla H, Tanner LB, Narayanaswamy P, Wenk MR, Nakatsu F, de Camilli P (2015). PI4P/phosphatidylserine countertransport at ORP5- and ORP8- mediated ER–plasma membrane contacts. Science 349, 428–432.

Coelho DS, Cairrão F, Zeng X, Pires E, Coelho AV, Ron D, Ryoo HD, Domingos PM (2013). Xbp1-independent Ire1 signaling is required for photoreceptor differentiation and rhabdomere morphogenesis in *Drosophila*. Cell Rep 5, 791–801.

Craige B, Salazar G, Faundez V (2008). Phosphatidylinositol-4-kinase type II alpha contains an AP-3–sorting motif and a kinase domain that are both required for endosome traffic. Mol Biol Cell 19, 1415–1426.

Del Bel LM, Brill JA (2018). Sac1, a lipid phosphatase at the interface of vesicular and nonvesicular transport. Traffic 19, 301–318.

Del Bel LM, Griffiths N, Wilk R, Wei H-C, Blagoveshchenskaya A, Burgess J, Polevoy G, Price JV, Mayinger P, Brill JA (2018). The phosphoinositide phosphatase Sac1 regulates cell shape and microtubule stability in the developing *Drosophila* eye. Development 145, dev151571.

Devergne O, Tsung K, Barcelo G, Schupbach T (2014). Polarized deposition of basement membrane proteins depends on phosphatidylinositol synthase and the levels of phosphatidylinositol 4,5-bisphosphate. Proc Natl Acad Sci 111, 7689–7694.

Diederich RJ, Matsuno K, Hing H, Artavanis-Tsakonas S (1994). Cytosolic interaction between deltex and Notch ankyrin repeats implicates deltex in the Notch signaling pathway. Development 120, 473–481.

Dong R, Saheki Y, Swarup S, Lucast L, Harper JW, De Camilli P (2016). Endosome-ER contacts control actin nucleation and retromer function through VAP-dependent regulation of PI4P. Cell 166, 408–423.

Donoviel DB, Freed DD, Vogel H, Potter DG, Hawkins E, Barrish JP, Mathur BN, Turner AC, Geske R, Montgomery CA, et al. (2001). Proteinuria and perinatal lethality in mice lacking NEPH1, a novel protein with homology to NEPHRIN. Mol Cell Biol 21, 4829–4836.

Fairn GD, McMaster CR (2008). Emerging roles of the oxysterol-binding protein family in metabolism, transport, and signaling. Cell Mol Life Sci 65, 228–236.

Faulhammer F, Kanjilal-Kolar S, Knödler A, Lo J, Lee Y, Konrad G, Mayinger P (2007). Growth control of Golgi phosphoinositides by reciprocal localization of Sac1 lipid phosphatase and Pik1 4-kinase. Traffic 8, 1554–1567.

Faulhammer F, Konrad G, Brankatschk B, Tahirovic S, Knödler A, Mayinger P (2005). Cell growth-dependent coordination of lipid signaling and glycosylation is mediated by interactions between Sac1p and Dpm1p. J Cell Biol 168, 185–191.

Fehon RG, Kooh PJ, Rebay I, Regan CL, Xu T, Muskavitch MAT, Artavanis-Tsakonas S (1990). Molecular interactions between the protein products of the neurogenic loci Notch and Delta, two EGF-homologous genes in *Drosophila*. Cell 61, 523–534.

Forrest S, Chai A, Sanhueza M, Marescotti M, Parry K, Georgiev A, Sahota V, Mendez-Castro R, Pennetta G (2013). Increased levels of phosphoinositides cause neurodegeneration in a *Drosophila* model of amyotrophic lateral sclerosis. Hum Mol Genet 22, 2689–2704.

Fujita E, Kouroku Y, Isoai A, Kumagai H, Misutani A, Matsuda C, Hayashi YK, Momoi T (2007). Two endoplasmic reticulum-associated degradation (ERAD) systems for the novel variant of the mutant dysferlin: Ubiquitin/

proteasome ERAD(I) and autophagy/lysosome ERAD(II). Hum Mol Genet 16, 618–629.

Godi A, Pertile P, Meyers R, Marra P, Di Tullio G, Iurisci C, Luini A, Corda D, De Matteis MA (1999). ARF mediates recruitment of PtdIns-4-OH kinase-β and stimulates synthesis of PtdIns(4,5)P_2 on the Golgi complex. Nat Cell Biol 1, 280–287.

Graham TR, Burd CG (2011). Coordination of Golgi functions by phosphatidylinositol 4-kinases. Trends Cell Biol 21, 113–121.

Hammond GRV, Machner MP, Balla T (2014). A novel probe for phosphatidylinositol 4-phosphate reveals multiple pools beyond the Golgi. J Cell Biol 205, 113–126.

Helmstädter M, Höhne M, Huber TB (2014). A brief overview on IRM function across evolution. J Neurogenet 28, 264–269.

Hofmann I, Munro S (2006). An N-terminally acetylated Arf-like GTPase is localised to lysosomes and affects their motility. J Cell Sci 119, 1494–1503.

Houck SA, Cyr DM (2012). Mechanisms for quality control of misfolded transmembrane proteins. Biochim Biophys Acta - Biomembr 1818, 1108–1114.

Jiang K, Liu Y, Fan J, Zhang J, Li XA, Evers BM, Zhu H, Jia J (2016). PI(4)P promotes phosphorylation and conformational change of Smoothened through interaction with its C-terminal tail. PLoS Biol 14, e1002375.

Johansson M, Rocha N, Zwart W, Jordens I, Janssen L, Kuijl C, Olkkonen VM, Neefjes J (2007). Activation of endosomal dynein motors by stepwise assembly of Rab7-RILP-p150^{Glued}, ORP1L, and the receptor βIII spectrin. J Cell Biol 176, 459–471.

Johnson DE, Ostrowski P, Jaumouillé V, Grinstein S (2016). The position of lysosomes within the cell determines their luminal pH. J Cell Biol 212, 677–692.

Johnston SA, May RC (2010). The human fungal pathogen Cryptococcus neoformans escapes macrophages by a phagosome emptying mechanism that is inhibited by Arp2/3 complex-mediated actin polymerisation. PLoS Pathog 6, e1001041.

Jordens I, Fernandez-Borja M, Marsman M, Dusseljee S, Janssen L, Calafat J, Janssen H, Wubbolts R, Neefjes J (2001). The Rab7 effector protein RILP controls lysosomal transport by inducing the recruitment of dynein-dynactin motors. Curr Biol 11, 1680–1685.

Jovic M, Kean MJ, Szentpetery Z, Polevoy G, Gingras A-C, Brill JA, Balla T (2012). Two phosphatidylinositol 4-kinases control lysosomal delivery of the Gaucher disease enzyme, β-glucocerebrosidase. Mol Biol Cell 23, 1533–1545.

Kochendorfer K-U, Then AR, Kearns BG, Bankaitis VA, Mayinger P (1999). Sac1p plays a crucial role in microsomal ATP transport, which is distinct from its function in Golgi phospholipid metabolism. EMBO J 18, 1506–1515.

Koponen A, Arora A, Takahashi K, Kentala H, Kivelä A, Jääskeläinen E, Peränen J, Somerharju P, Ikonen E, Viitala T, et al. (2018). ORP2 interacts with phosphoinositides and controls the subcellular distribution of cholesterol. Biochimie 158, 90–101.

Lee AS (2005). The ER chaperone and signaling regulator GRP78/BiP as a monitor of endoplasmic reticulum stress. Methods 35, 373–381.

Lee S, Kim S, Nahm M, Kim E, Kim TII, Yoon JH, Lee S (2011). The phosphoinositide phosphatase Sac1 is required for midline axon guidance. Mol Cells 32, 477–482.

Lehto M, Laitinen S, Chinetti G, Johansson M, Ehnholm C, Staels B, Ikonen E, Olkkonen VM (2001). The OSBP-related protein family in humans. J Lipid Res Res 42, 1203–1213.

Lev S (2010). Non-vesicular lipid transport by lipid-transfer proteins and beyond. Nat Rev Mol Cell Biol 11, 739–750.

Levin R, Hammond GRV, Balla T, De Camilli P, Fairn GD, Grinstein S (2017). Multiphasic dynamics of phosphatidylinositol 4-phosphate during phagocytosis. Mol Biol Cell 28, 128–140.

Levine TP, Munro S (2002). Targeting of Golgi-specific pleckstrin homology domains involves both PtdIns 4-kinase-dependent and -independent components. Curr Biol 12, 695–704.

Liebl D, Griffiths G (2009). Transient assembly of F-actin by phagosomes delays phagosome fusion with lysosomes in cargo-overloaded macrophages. J Cell Sci 122, 2935–2945.

Liu X, Ridgway ND (2014). Characterization of the sterol and phosphatidylinositol 4-phosphate binding properties of Golgi-associated OSBP-related protein 9 (ORP9). PLoS One 9, e108368.

Loewen CJR, Roy A, Levine TP (2003). A conserved ER targeting motif in three families of lipid binding proteins and in Opi1p binds VAP. EMBO J 22, 2025–2035.

Longley RL, Ready DF (1995). Integrins and the development of three-dimensional structure in the Drosophila compound eye. Dev Biol 171, 415–433.

Ma Z, Liu Z, Huang X (2010). OSBP- and FAN-mediated sterol requirement for spermatogenesis in Drosophila. Development 137, 3775–3784.

Ma CIJ, Yang Y, Kim T, Chen CH, Polevoy G, Vissa M, Burgess J, Brill JA (2020). An early endosome-derived retrograde trafficking pathway promotes secretory granule maturation. J Cell Biol 219, e201808017.

Machado MCR, Octacilio-Silva S, Costa MSA, Ramos RGP (2011). rst transcriptional activity influences kirre mRNA concentration in the Drosophila pupal retina during the final steps of ommatidial patterning. PLoS One 6, e22536.

Manford A, Xia T, Saxena AK, Stefan C, Hu F, Emr SD, Mao Y (2010). Crystal structure of the yeast Sac1: Implications for its phosphoinositide phosphatase function. EMBO J 29, 1489–1498.

Mao D, Lin G, Tepe B, Zuo Z, Tan KL, Senturk M, Zhang S, Arenkiel BR, Sardiello M, Bellen HJ (2019). VAMP associated proteins are required for autophagic and lysosomal degradation by promoting a PtdIns4P-mediated endosomal pathway. Autophagy 15, 1214–1233.

Marois E, Mahmoud A, Eaton S (2006). The endocytic pathway and formation of the Wingless morphogen gradient. Development 133, 307–317.

Marquer C, Tian H, Yi J, Bastien J, Dall'Armi C, Yang-Klingler Y, Zhou B, Chan RB, Di Paolo G (2016). Arf6 controls retromer traffic and intracellular cholesterol distribution via a phosphoinositide-based mechanism. Nat Commun 7, 11919.

Mayinger P, Bankaitis VA, Meyer DI (1995). Sac1p mediates the adenosine triphosphate transport into yeast endoplasmic reticulum that is required for protein translocation. J Cell Biol 131, 1377–1386.

Mesmin B, Bigay J, Moser Von Filseck J, Lacas-Gervais S, Drin G, Antonny B (2013). A four-step cycle driven by PI(4)P hydrolysis directs sterol/PI(4)P exchange by the ER-Golgi tether OSBP. Cell 155, 830–843.

Mesmin B, Bigay J, Polidori J, Jamecna D, Lacas Gervais S, Antonny B (2017). Sterol transfer, PI4P consumption, and control of membrane lipid order by endogenous OSBP. EMBO J 36, 3156–3174.

Minogue S, Waugh MG, De Matteis MA, Stephens DJ, Berditchevski F, Hsuan JJ (2006). Phosphatidylinositol 4-kinase is required for endosomal trafficking and degradation of the EGF receptor. J Cell Sci 119, 571–581.

Minogue S, Chu KME, Westover EJ, Covey DF, Hsuan JJ, Waugh MG (2010). Relationship between phosphatidylinositol 4-phosphate synthesis, membrane organization, and lateral diffusion of PI4KIIα at the trans-Golgi network. J Lipid Res 51, 2314–2324.

Moustaqim-Barrette A, Lin YQ, Pradhan S, Neely GG, Bellen HJ, Tsuda H (2014). The amyotrophic lateral sclerosis 8 protein, VAP, is required for ER protein quality control. Hum Mol Genet 23, 1975–1989.

Nakatsu F, Baskin JM, Chung J, Tanner LB, Shui G, Lee SY, Pirruccello M, Hao M, Ingolia NT, Wenk MR, et al. (2012). PtdIns4P synthesis by PI4KIIIα at the plasma membrane and its impact on plasma membrane identity. J Cell Biol 199, 1003–1016.

Nezis IP, Simonsen A, Sagona AP, Finley K, Gaumer S, Contamine D, Rusten TE, Stenmark H, Brech A (2008). Ref(2)P, the Drosophila melanogaster homologue of mammalian p62, is required for the formation of protein aggregates in adult brain. J Cell Biol 180, 1065–1071.

Oda H, Uemura T, Harada Y, Iwai Y, Takeichi M (1994). A Drosophila homolog of Cadherin associated with Armadillo and essential for embryonic cell-cell adhesion. Dev Biol 165, 716–726.

Otero JH, Lizak B, Hendershot LM (2010). Life and death of a BiP substrate. Semin Cell Dev Biol 21, 472–478.

Parnas D, Haghighi AP, Fetter RD, Kim SW, Goodman CS (2001). Regulation of postsynaptic structure and protein localization by the Rho-type guanine nucleotide exchange factor dPix. Neuron 32, 415–424.

Pellikka M, Tanentzapf G, Pinto M, Smith C, McGlade CJ, Ready DF, Tepass U (2002). Crumbs, the Drosophila homologue of human CRB1/RP12, is essential for photoreceptor morphogenesis. Nature 416, 143–149.

Pietrangelo A, Ridgway ND (2018). Bridging the molecular and biological functions of the oxysterol-binding protein family. Cell Mol Life Sci 75, 3079–3098.

Polevoy G, Wei HC, Wong R, Szentpetery Z, Kim YJ, Goldbach P, Steinbach SK, Balla T, Brill JA (2009). Dual roles for the Drosophila PI 4-kinase Four wheel drive in localizing Rab11 during cytokinesis. J Cell Biol 187, 847–858.

Pulipparacharuvil S, Akbar MA, Ray S, Sevrioukov EA, Haberman AS, Rohrer J, Kramer H (2005). Drosophila Vps16A is required for trafficking to lysosomes and biogenesis of pigment granules. J Cell Sci 118, 3663–3673.

Ready DF, Hanson TE, Benzer S (1976). Development of the Drosophila retina, a neurocrystalline lattice. Dev Biol 53, 217–240.

Reiter C, Schimansky T, Nie Z, Fischbach KF (1996). Reorganization of membrane contacts prior to apoptosis in the *Drosophila* retina: the role of the IrreC-rst protein. Development 122, 1931–1940.

Riedel F, Gillingham AK, Rosa-Ferreira C, Galindo A, Munro S (2016). An antibody toolkit for the study of membrane traffic in *Drosophila melanogaster*. Biol Open 5, 987–992.

Riggleman B, Schedl P, Wieschaus E (1990). Spatial expression of the *Drosophila* segment polarity gene *armadillo* is posttranscriptionally regulated by *wingless*. Cell 63, 549–560.

Rocha N, Kuijl C, Van Der Kant R, Janssen L, Houben D, Janssen H, Zwart W, Neefjes J (2009). Cholesterol sensor ORP1L contacts the ER protein VAP to control Rab7-RILP-p150[Glued] and late endosome positioning. J Cell Biol 185, 1209–1225.

Rosa-Ferreira C, Sweeney ST, Munro S (2018). The small G protein Arl8 contributes to lysosomal function and long-range axonal transport in *Drosophila*. Biol Open 7, bio035964.

Ruiz-Gómez M, Coutts N, Price A, Taylor MV, Bate M (2000). *Drosophila* Dumbfounded: A myoblast attractant essential for fusion. Cell 102, 189–198.

Ruotsalainen V, Ljungberg P, Wartiovaara J, Lenkkeri U, Kestila M, Jalanko H, Holmberg C, Tryggvason K (1999). Nephrin is specifically located at the slit diaphragm of glomerular podocytes. Proc Natl Acad Sci 96, 7962–7967.

Salazar G, Craige B, Wainer BH, Guo J, De Camilli P, Faundez V (2005). Phosphatidylinositol-4-kinase type IIα is a component of adaptor protein-3-derived vesicles. Mol Biol Cell 16, 3692–3704.

Schneider T, Reiter C, Eule E, Bader B, Lichte B, Nie Z, Schimansky T, Ramos RGP, Fischbach KF (1995). Restricted expression of the irreC-rst protein is required for normal axonal projections of columnar visual neurons. Neuron 15, 259–271.

Şentürk M, Lin G, Zuo Z, Mao D, Watson E, Mikos AG, Bellen HJ (2019). Ubiquilins regulate autophagic flux through mTOR signalling and lysosomal acidification. Nat Cell Biol 21, 384–396.

Sisson JC, Field C, Ventura R, Royou A, Sullivan W (2000). Lava lamp, a novel peripheral Golgi protein, is required for *Drosophila melanogaster* cellularization. J Cell Biol 151, 905–917.

Sohn M, Korzeniowski M, Zewe JP, Wills RC, Hammond GRV, Humpolickova J, Vrzal L, Chalupska D, Veverka V, Fairn GD, *et al.* (2018). PI(4,5)P₂ controls plasma membrane PI4P and PS levels via ORP5/8 recruitment to ER – PM contact sites. J Cell Biol 217, 1797–1813.

Sohn RL, Huang P, Kawahara G, Mitchell M, Guyon J, Kalluri R, Kunkel LM, Gussoni E (2009). A role for nephrin, a renal protein, in vertebrate skeletal muscle cell fusion. Proc Natl Acad Sci 106, 9274–9279.

Sone M, Zeng X, Larese J, Ryoo HD (2013). A modified UPR stress sensing system reveals a novel tissue distribution of IRE1/XBP1 activity during normal *Drosophila* development. Cell Stress Chaperon 18, 307–319.

Stefan CJ, Manford AG, Baird D, Yamada-Hanff J, Mao Y, Emr SD (2011). Osh proteins regulate phosphoinositide metabolism at ER-plasma membrane contact sites. Cell 144, 389–401.

Strünkelnberg M, Bonengel B, Moda LM, Hertenstein A, de Couet HG, Ramos RG, Fischbach KF (2001). *rst* and its paralogue *kirre* act redundantly during embryonic muscle development in Drosophila. Development 128, 4229–4239.

Tan J, Oh K, Burgess J, Hipfner DR, Brill JA (2014). PI4KIIIα is required for cortical integrity and cell polarity during *Drosophila* oogenesis. J Cell Sci 127, 954–966.

Tan J, Brill JA (2014). Cinderella story: PI4P goes from precursor to key signaling molecule. Crit Rev Biochem Mol Biol 49, 33–58.

Tomlinson A (1985). The cellular dynamics of pattern formation in the eye of *Drosophila*. J Embryol Exp Morphol 89, 313–331.

Tomlinson A (2012). The origin of the *Drosophila* subretinal pigment layer. J Comp Neurol 520, 2676–2682.

Tomlinson A, Ready DF (1987). Neuronal differentiation in the *Drosophila* ommatidium. Dev Biol 120, 366–376.

Tryggvason K (1999). Unraveling the mechanisms of glomerular ultrafiltration: Nephrin, a key component of the slit diaphragm. J Am Soc Nephrol 10, 2440–2445.

Tsuda H, Han SM, Yang Y, Tong C, Lin YQ, Mohan K, Haueter C, Zoghbi A, Harati Y, Kwan J, *et al.* (2008). The Amyotrophic lateral sclerosis 8 protein VAPB is cleaved, secreted, and acts as a ligand for Eph receptors. Cell 133, 963–977.

van der Kant R, Fish A, Janssen L, Janssen H, Krom S, Ho N, Brummelkamp T, Carette J, Rocha N, Neefjes J (2013). Late endosomal transport and tethering are coupled processes controlled by RILP and the cholesterol sensor ORP1L. J Cell Sci 126, 3462–3474.

Venditti R, Masone MC, Rega LR, Tullio GDi, Santoro M, Polishchuk E, Serrano IC, Olkkonen VM, Harada A, Medina DL, *et al.* (2019a). The activity of Sac1 across ER–TGN contact sites requires the four-phosphate-adaptor-protein-1. J Cell Biol 218, 783–797.

Venditti R, Rega LR, Masone MC, Santoro M, Polishchuk E, Sarnataro D, Paladino S, Auria SD, Varriale A, Olkkonen VM, *et al.* (2019b). Molecular determinants of ER–Golgi contacts identified through a new FRET–FLIM system. J Cell Biol 218, 1055–1065.

Vihervaara T, Uronen R-L, Wohlfahrt G, Björkhem I, Ikonen E, Olkkonen VM (2011). Sterol binding by OSBP-related protein 1L regulates late endosome motility and function. Cell Mol Life Sci 68, 537–551.

Walch-Solimena C, Novick P (1999). The yeast phosphatidylinositol-4-OH kinase Pik1 regulates secretion at the Golgi. Nat Cell Biol 1, 523–525.

Wallroth A, Haucke V (2018). Phosphoinositide conversion in endocytosis and the endolysosomal system. J Biol Chem 293, 1526–1535.

Walther RF, Pichaud F (2006). Immunofluorescent staining and imaging of the pupal and adult *Drosophila* visual system. Nat Protoc 1, 2635–2642.

Wang H, Ma Q, Qi Y, Dong J, Du X, Rae J, Wang J, Wu W-F, Brown AJ, Parton RG, *et al.* (2019). ORP2 delivers cholesterol to the plasma membrane in exchange for phosphatidylinositol 4, 5-bisphosphate (PI(4,5)P₂). Mol Cell 73, 458–473.

Wang YJ, Wang J, Sun HQ, Martinez M, Sun YX, Macia E, Kirchhausen T, Albanesi JP, Roth MG, Yin HL (2003). Phosphatidylinositol 4 phosphate regulates targeting of clathrin adaptor AP-1 complexes to the Golgi. Cell 114, 299–310.

Wei HC, Sanny J, Shu H, Baillie DL, Brill JA, Price JV, Harden N (2003a). The Sac1 lipid phosphatase regulates cell shape change and the JNK cascade during dorsal closure in *Drosophila*. Curr Biol 13, 1882–1887.

Wei H-C, Shu H, Price JV (2003b). Functional genomic analysis of the 61D-61F region of the third chromosome of *Drosophila melanogaster*. Genome 46, 1049–1058.

Wijdeven RH, Janssen H, Nahidiazar L, Janssen L, Jalink K, Berlin I, Neefjes J (2016). Cholesterol and ORP1L-mediated ER contact sites control autophagosome transport and fusion with the endocytic pathway. Nat Commun 7, 11808.

Wolff T (2000). Histological techniques for the *Drosophila* eye. Part II: Adult. In: *Drosophila* protocols, ed. W Sullivan, M Ashburner, and RS Hawley, Cold Spring Harbor, NY: Cold Spring Harbor Press, 229–244.

Wolff T, Ready DF (1991). Cell death in normal and rough eye mutants of *Drosophila*. Development 113, 825–839.

Wooten MW, Hu X, Babu JR, Seibenhener ML, Geetha T, Paine MG, Wooten MC (2006). Signaling, polyubiquitination, trafficking, and inclusions: Sequestosome 1/p62's role in neurodegenerative disease. J Biomed Biotechnol 62079.

Wucherpfennig T, Wilsch-Bräuninger M, González-Gaitán M (2003). Role of *Drosophila* Rab5 during endosomal trafficking at the synapse and evoked neurotransmitter release. J Cell Biol 161, 609–624.

Wyles JP, McMaster CR, Ridgway ND (2002). Vesicle-associated membrane protein-associated protein-A (VAP-A) interacts with the oxysterol-binding protein to modify export from the endoplasmic reticulum. J Biol Chem 277, 29908–29918.

Xu T, Rubin GM (1993). Analysis of genetic mosaics in developing and adult *Drosophila* tissues. Development 117, 1223–1237.

Yan Y, Denef N, Tang C, Schüpbach T (2011). *Drosophila* PI4KIIIalpha is required in follicle cells for oocyte polarization and Hippo signaling. Development 138, 1697–1703.

Yavari A, Nagaraj R, Owusu-Ansah E, Folick A, Ngo K, Hillman T, Call G, Rohatgi R, Scott MP, Banerjee U (2010). Role of lipid metabolism in Smoothened derepression in Hedgehog signaling. Dev Cell 19, 54–65.

Zhao K, Ridgway ND (2017). Oxysterol-binding protein-related protein 1L regulates cholesterol egress from the endo-lysosomal system. Cell Rep 19, 1807–1818.

Zusman S, Grinblat Y, Yee G, Kafatos FC, Hynes RO (1993). Analyses of PS integrin functions during *Drosophila* development. Development 118, 737–750.